

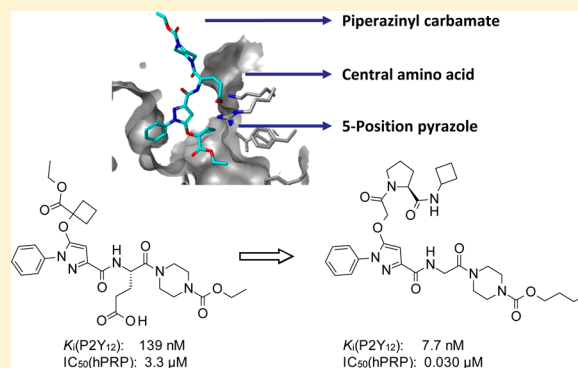
Identification of High-Affinity P2Y₁₂ Antagonists Based on a Phenylpyrazole Glutamic Acid Piperazine Backbone

Gernot Zech, Gerhard Hessler, Andreas Evers, Tilo Weiss, Peter Florian, Melitta Just, Jörg Czech, Werngard Czechtizky, Jochen Görlitzer, Sven Ruf, Markus Kohlmann, and Marc Nazaré*

Sanofi-Aventis Deutschland GmbH, Industriepark Höchst, Building G878, D-65926 Frankfurt am Main, Germany

Supporting Information

ABSTRACT: A series of novel, highly potent P2Y₁₂ antagonists as inhibitors of platelet aggregation based on a phenylpyrazole glutamic acid piperazine backbone is described. Exploration of the structural requirements of the substituents by probing the structure–activity relationship along this backbone led to the discovery of the *N*-acetyl-(*S*)-proline cyclobutyl amide moiety as a highly privileged motif. Combining the most favorable substituents led to remarkably potent P2Y₁₂ antagonists displaying not only low nanomolar binding affinity to the P2Y₁₂ receptor but also a low nanomolar inhibition of platelet aggregation in the human platelet rich plasma assay with IC₅₀ values below 50 nM. Using a homology and a three-dimensional quantitative structure–activity relationship model, a binding hypothesis elucidating the impact of several structural features was developed.



1. INTRODUCTION

The activation and aggregation of blood platelets are essential for normal hemostasis but are also key mechanisms for triggering acute, potentially life-threatening arterial thrombotic events like myocardial infarction or thromboembolic stroke. In this context, adenosine-5'-diphosphate (ADP) is a central signaling molecule inducing platelet activation and aggregation, thus playing a key role in the initiation and progression of arterial thrombus formation. Upon activation by various stimuli, like collagen (Col) and thrombin (Thr), ADP is released from blood platelets in the vasculature, as well as from damaged blood cells, endothelium, or tissues.¹ The ADP-induced platelet aggregation is triggered by its binding to two specific G-protein-coupled receptors (GPCRs), P2Y purinoceptor 1 (P2Y₁) and P2Y purinoceptor 12 (P2Y₁₂), which are expressed on the plasma membrane of human platelets. ADP binding to these receptors induces inhibition of adenylyl cyclase and modulation of intracellular signaling pathways such as influx and mobilization of intracellular Ca²⁺, activation of phosphoinositide-3 kinase (PI3K), shape change, platelet aggregation, and secretion of other mediators, thus amplifying the initial proaggregatory signal.² In particular the P2Y₁₂ receptor has been recognized as a highly attractive target, as its activation is required for platelet secretion and stabilization of platelet aggregates, and in contrast to the ubiquitously expressed P2Y₁ receptor, the P2Y₁₂ receptor is mainly expressed on platelets.³ Moreover, experimental studies have shown that sole inhibition of the P2Y₁₂ receptor is sufficient to block and prevent platelet aggregation.⁴

The widespread successful clinical use of the irreversible P2Y₁₂ antagonist clopidogrel⁵ has demonstrated the high impact and relevance of inhibiting this mechanism for the prevention of thrombotic complications of atherosclerosis. Albeit being highly selective, clopidogrel requires hepatic metabolic conversion to an active metabolite that covalently modifies the P2Y₁₂ receptor, which results in a slow onset and offset of its pharmacological action.⁶ Consequently, extensive drug discovery efforts were made to identify potent, direct-acting, and reversible P2Y₁₂ antagonists resulting in promising compounds like Ticagrelor (AZD-6140) (1),⁷ Elinogrel (PRT-128) (2),⁸ and BX 667 (3)⁹ (Chart 1).

The activity data for the majority of reversible antagonists show that, despite high binding affinity to the P2Y₁₂ receptor, the inhibitory activity in the clinical relevant functional human platelet-rich plasma (hPRP) assay, which is a key predictor for the antithrombotic pharmacological effect,¹⁰ still leaves significant room for improvement. For example, when evaluating the antiaggregatory activity in hPRP of 1–3 in our standard assay system, which was used throughout this investigation, potencies in the micromolar range were determined. However, improving the P2Y₁₂-mediated inhibitory potency in the hPRP assay setting remains a significant challenge as the observed activity is governed by the complex interplay of several parameters such as receptor binding affinity, plasma protein binding, and polarity of the antagonist.¹¹

Received: June 4, 2012

Published: September 17, 2012

Chart 1. Structures of 1 (Ticagrelor), 2 (Elinogrel), and 3 (BX 667) and Their Respective Affinity in the P2Y₁₂ Binding Assay and Antiaggregatory Activity in the Human Platelet-Rich Plasma (hPRP) Assay Used Throughout This Investigation (See the Experimental Section)

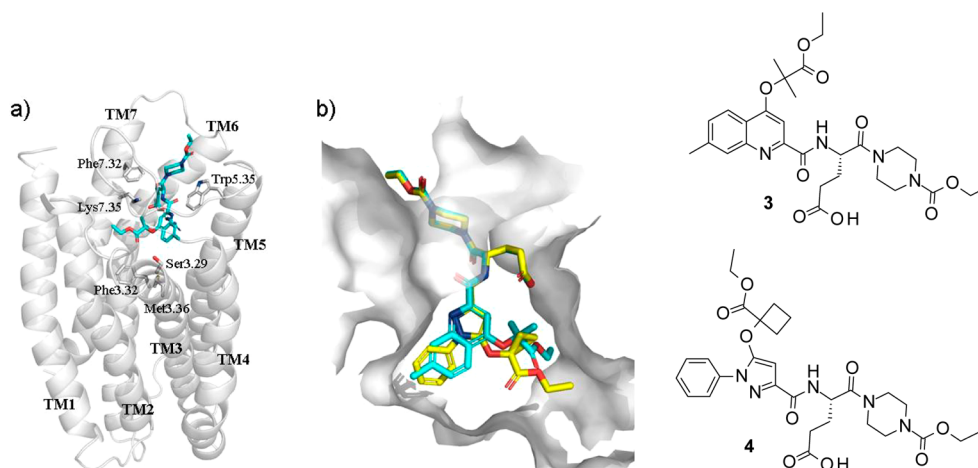
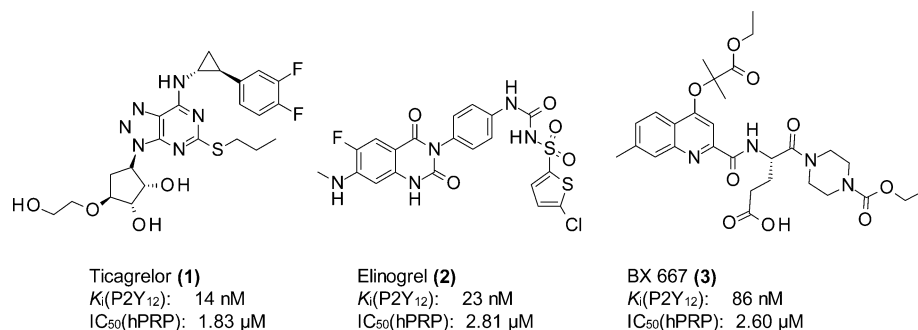


Figure 1. (a) Binding hypothesis of quinoline **3** in the P2Y₁₂ receptor obtained from docking into a receptor homology model. (b) Three-dimensional alignment of quinoline **3** and phenylpyrazolone **4**.

In seeking suitable P2Y₁₂ drug candidates in this area, we¹² along with others^{9,11,13} have explored glutamic acid piperazine derivatives as reversible P2Y₁₂ antagonists. Here, we report our findings on the identification of novel, highly potent P2Y₁₂ antagonists based on a phenylpyrazolone scaffold and the discovery of new high-affinity ligand substitution patterns resulting in a dramatic enhancement in binding affinity and functional activity.

2. RESULTS AND DISCUSSION

2.1. Identification of the Phenylpyrazolone Scaffold by Structure-Based Alignment Studies. As a result of initial alignment considerations in the context of P2Y₁₂ antagonists of the glutamic acid piperazine type, we anticipated that a phenylpyrazolone scaffold¹² as shown in compound **4** could be a suitable replacement for the initial quinoline scaffold in compound **3** (Figure 1). To further rationalize our ligand design efforts and direct our structure–activity relationship (SAR) investigation, we intended to use structure-based alignments. However, although tremendous progress has been made in revealing 3D structures of GPCRs, the investigation of 3D structures of membrane proteins remains a significant challenge, and there is currently no P2Y₁₂ X-ray crystal structure available. Therefore, we resorted to the use of homology modeling to gain structural insights into protein–ligand interactions for P2Y₁₂. For the generation of binding hypotheses, a homology model of the P2Y₁₂ receptor was created using the crystal structure of the C-X-C chemokine

receptor type 4 (CXCR4) receptor as a structural template (see the Experimental Section), which had previously been identified as the most-suited structural template.¹⁴ Two main factors limit the accuracy of the P2Y₁₂ protein model, namely, the relatively low sequence identity of 25.6% in the transmembrane region and the diverse orientations of the extracellular 2 (EC2) loop linked to transmembrane helix 3 (TM3) by a cysteine bridge. On the basis of the analysis of different GPCR crystal structures, it has been shown that residues from this loop region participate in ligand binding in different GPCRs.¹⁵ Consequently, we had to take into account that the EC2 loop orientation is different from that observed in the CXCR4 template. To compensate for these factors, limiting the accuracy of the protein model, we cross-checked the docking mode with available mutagenesis and ligand SAR data. Furthermore, we used the docking modes of quinoline lead **3** and phenylpyrazolone **4** as the structural basis for the generation of multiple ligand alignments and derivation of ligand-based 3D quantitative structure–activity relationship (QSAR) models.

Figure 1a shows the binding hypothesis for **3**, which was obtained from molecular docking into our homology model of the P2Y₁₂ receptor. The quinoline lead **3** binds into a cavity formed by residues from TM3, TM4, TM5, TM6, and TM7. The carboxy group is coordinated by the basic side chains of residues Arg6.55 and Lys7.35. Whereas the docking mode proposes a localization of the 4-hydroxy-quinoline moiety in a hydrophobic subpocket, the piperazinyl carbamate substituent

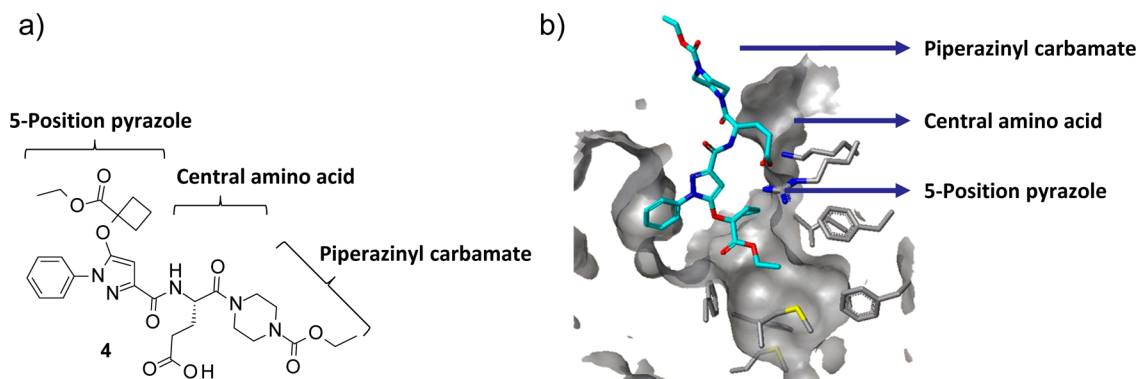


Figure 2. (a) Schematic representation of the regions to be investigated based on the phenylpyrazolone backbone. (b) Proposed binding mode of pyrazole 4 into the P2Y₁₂ homology model.

points toward the extracellular region. Interestingly, a similar docking hypothesis was recently described for a related chemical series of piperazinyl glutamic acid pyrimidines.¹⁶ Pyrazole 4 was docked in to the P2Y₁₂ homology model as well (Figure 1b). As shown, the large identical glutamic acid piperazinyl carbamate fragments align well. The phenylpyrazolone moiety is placed in the same hydrophobic pocket as the quinoline fragment. However, a more careful inspection of the 3D alignment of 3 with 4 reveals that the substituent at the 5-position of the pyrazole 4 does not align with the corresponding substituent at the 4-position of the quinoline 3 (see Figure 1b). Thus, the substantial topological change from the quinoline to the pyrazole scaffold obviously also required an examination of the remaining regions of the ligand.

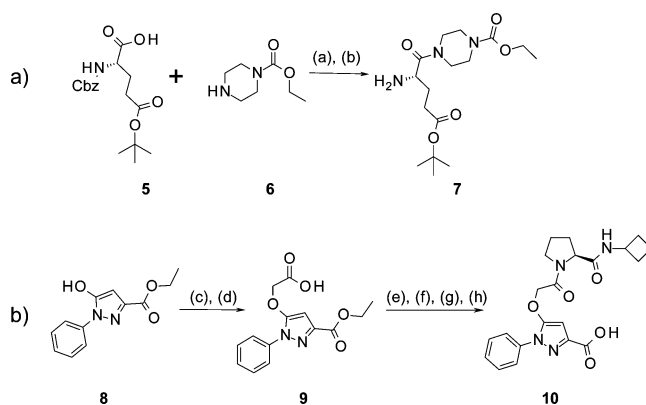
Figure 2a gives a schematic representation of the regions that we intended to explore based on the phenylpyrazolone glutamic acid piperazine backbone. Analysis of the docking mode of pyrazole 4 (Figure 2b) suggested that in particular the 5-position of the pyrazole should be a promising region for further variations. Consequently, we first set out to systematically probe the influence of variations at the 5-position of the phenylpyrazole. The glutamic acid side chain was kept constant throughout these initial variations serving as a strong mediator of affinity for the putative antagonists.

3. CHEMISTRY

Scheme 1 shows the synthesis of representative building blocks, which were sequentially attached to the 3-carboxyphenylpyrazole, enabling a highly convergent and flexible synthesis of the final ligands. The glutamic piperazinyl carbamate building block 7 was prepared from the commercially available *Z*-*O*-*tert*-butyl protected 5 in two steps by standard amide coupling using *O*-((ethoxycarbonyl)cyanomethyleneamino)-*N,N,N',N'*-tetramethyluronium tetrafluoroborate (TOTU) followed by the hydrogenolytic removal of the Cbz-protecting group (sequence a). The second key intermediate used throughout this investigation was the fully decorated phenylpyrazole building block 10 (sequence b). This fragment was synthesized by subjecting the phenylpyrazole ester 8 to an *O*-alkylation with benzyl 2-bromoacetate followed by selective hydrogenolytic cleavage of the benzylester to give 9. This intermediate was then converted to the acid 10 by a high-yielding sequence of amide coupling and deprotection steps.

The syntheses of the fully decorated final phenylpyrazolone ligands with different substituents attached to the 5-position of the pyrazole and all other side chain variations were carried out

Scheme 1. Synthetic Routes to Key Building Blocks^a

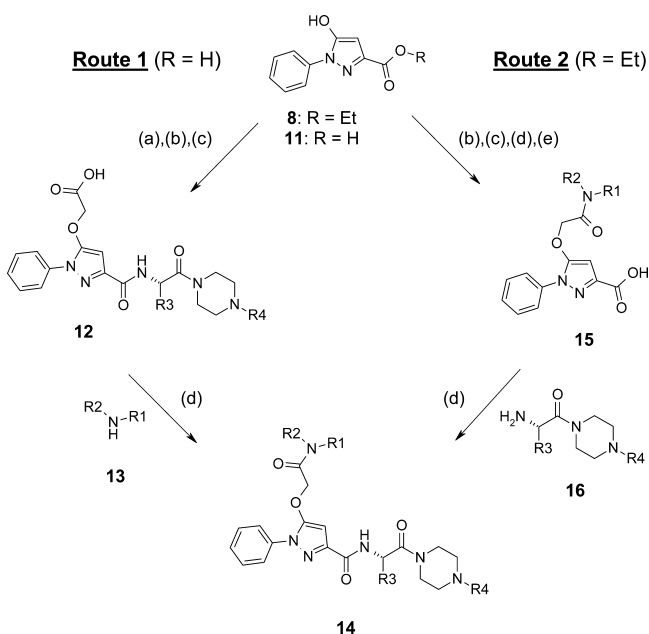


^aReagents and conditions: (a) TOTU, *N*-ethylmorpholine, DMF, room temp, 16 h, 90%. (b) H₂ (3 bar), Pd/C (10%), ethanol, room temp, 6 h, 90%. (c) Benzyl 2-bromoacetate, Cs₂CO₃, DMF, room temp, 12 h, 95%. (d) H₂ (3 bar), Pd/C (10%), EtOAc, room temp, 6 h, 76%. (e) Benzyl (2*S*)-pyrrolidine-2-carboxylate, EDC, HOBt, EtNiPr₂, DMF, room temp, 16 h, 84%. (f) H₂ (3 bar), Pd/C (10%), EtOAc, room temp, 6 h, 98%. (g) Cyclobutyl amine, HATU, EtNiPr₂, DMF, room temp, 16 h, 95%. (h) NaOH, H₂O/THF, room temp, 16 h, 95%.

by two optional routes starting from commercially available 3-carboxy phenyl pyrazolones 8 and 11 (Scheme 2).

Phenylpyrazolone variations keeping the piperazinyl side chain constant were synthesized according to route 1. Phenylpyrazolones of type 14 were prepared by using standard amide coupling conditions with 1-ethyl-3-(3-dimethylaminopropyl)carbodiimide hydrochloride (EDC)/1-hydroxybenzotriazole (HOBt) followed by *O*-alkylation of the phenylpyrazole with benzyl 2-bromoacetate in the presence of cesium carbonate in DMF and hydrogenolytic deprotection to the carboxylic acid 12. The diversifying amide variation step was then conducted using EDC/HOBt or *O*-(7-azabenzotriazol-1-yl)-*N,N,N',N'*-tetramethyluronium hexafluorophosphate (HATU) in DMF as activating reagents.

Route 2 was used to explore the impact of other side chain variations retaining the 5-*O*-alkyl amide substituent. The preassembled phenylpyrazole 15 and the piperazinyl side chain 16 were prepared according to the synthetic sequences outlined for the respective building blocks (Scheme 1, synthesis of 7 and 10) and then coupled using either EDC/HOBt or HATU activation in DMF to give the final derivatives 14. By using these synthetic routes, we were able to systematically

Scheme 2. Synthetic Routes Used for the Assembly of the Final P2Y₁₂ Antagonists^a

^aReagents and conditions: (a) EDC, HOBt, EtNiPr₂, **16**, DMF, room temp. (b) Benzyl 2-bromoacetate, Cs₂CO₃, DMF, room temp. (c) H₂ (3 bar), Pd/C (10%), EtOAc, room temp. (d) EDC, HOBt, EtNiPr₂, DMF, room temp or HATU, EtNiPr₂, DMF, room temp. (e) NaOH, H₂O/THF, room temp.

synthesize a wide range of P2Y₁₂ antagonists and to obtain a dense set of SAR data, which revealed key features of favorable and unfavorable interactions.

3. RESULTS AND DISCUSSION

The binding affinity of the compounds was determined by a human P2Y₁₂ receptor binding assay employing [³³P]2-MeS-ADP as the radioligand and human P2Y₁₂ transfected Chinese hamster ovary (CHO) cell membranes.¹⁷ The inhibitory effect on the ADP-stimulated platelet aggregation was determined *in vitro* in hPRP using a turbidimetric method in a 96-well format. For several compounds, the antiaggregatory activity was additionally confirmed as indicated in a second hPRP assay, the clinically relevant “Born method” using single cuvettes.¹⁰ Table 1 shows the SAR of an initial explorative library intended to examine the effects of various ester, ketone, and amide derivatizations obtained by route 1 transformations.

This survey illustrated the fact that the receptor recognition was highly sensitive to modifications at the 5-position of the pyrazole, which—according to our docking hypothesis—points into a buried subpocket composed of several hydrophobic amino acid side chains (see Figure 2b). Consequently, lipophilic substituents were preferred, and certain steric requirements existed to fill the lipophilic environment. This observation was also captured by the steric fields of the comparative molecular similarity index analysis (CoMSIA) model used to analyze the ligand data. (Figure 3). Having no substituent at the 5-position as in pyrazole **17a** (R = H) resulted in an essentially inactive compound and pinpointed the necessity for further substitution in this region. Introduction of substituted alkyl esters like **4** or **17b** or isosteric lipophilic ketones **17c**, **17d**, or **17e** were effective to obtain significant binding affinity and hPRP activity in the range of 2 μM. In

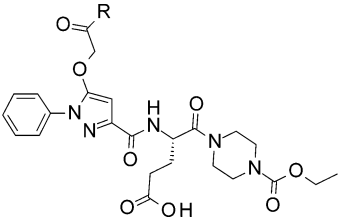
Table 1. Binding and hPRP Activity of Explorative Variations around the Initial Hit **4**

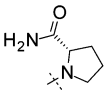
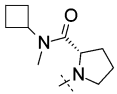
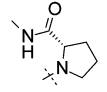
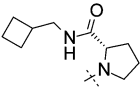
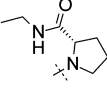
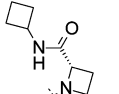
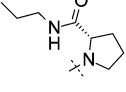
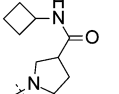
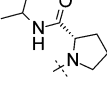
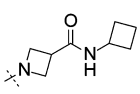
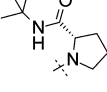
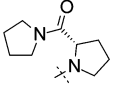
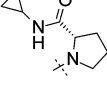
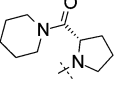
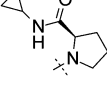
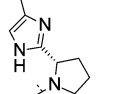
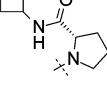
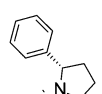
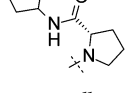
Compd	R	K _i (P2Y ₁₂) ^a (nM)	IC ₅₀ (hPRP) ^{b,c} (μM)
17a	H	>5000	>10
4		139	3.3 (2.93)
17b		372	2.25 (2.48)
17c		242	3.73 (2.46)
17d		249	2.60 (2.51)
17e		574	7.41
17f		2720	9.05
17g		>5000	>10
17h		459	1.37
17i		173	0.90

^aP2Y₁₂ binding assay using cell membranes from CHO cells with recombinant expression of human P2Y₁₂ receptors employing [³³P]2-MeS-ADP as the radioligand. ^bAntiaggregatory effect on ADP-stimulated hPRP using a 96-well format. ^cIn parentheses: Antiaggregatory effect on ADP-stimulated hPRP according to the Born method using single cuvettes.

contrast, the simple primary amide **17f** or the acyclic tertiary amide **17g** did not improve the activity but were significantly less active. Interestingly, when cyclic pyrrolidine amides were attached to the 5-position of the pyrazole instead (**17h**, **17i**), the most active compounds of this first survey were obtained reaching up to submicromolar potency in the hPRP assay [IC₅₀ (hPRP): 1.37 and 0.9 μM for **17h** and **17i**]. With this first evidence that cyclic amides could considerably enhance the ligand affinity and in particular the potency in the hPRP assay and with the aim to avoid the imide functionality present in **17i**,

Table 2. Binding and hPRP Activity of Compounds Carrying Various Proline Variations



Compd	R	$K_i(\text{P2Y}_{12})^a$ (nM)	$\text{IC}_{50}(\text{hPRP})^{b,c}$ (μM)	Compd	R	$K_i(\text{P2Y}_{12})^a$ (nM)	$\text{IC}_{50}(\text{hPRP})^{b,c}$ (μM)
18a		283	3.10	18k		27	0.22
18b		536	1.46	18l		19	0.100 (0.072)
18c		303	0.475	18m		42	0.076
18d		66	0.058 (0.091)	18n		238	3.13
18e		56	0.040	18o		613	2.94
18f		41	0.017 (0.070)	18p		219	0.60
18g		105	0.013	18q		56	0.070 (0.073)
18h		958	n.d.	18r		56	0.38
18i		7.3	0.025 (0.009)	18s		33	0.29
18j		20	0.013 (0.038)				

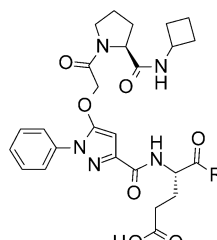
^aP2Y₁₂ binding assay using cell membranes from CHO cells with recombinant expression of human P2Y₁₂ receptors employing [³³P]2-MeS-ADP as the radioligand. ^bAntiaggregatory effect on ADP-stimulated hPRP using a 96-well format. ^cIn parentheses: Antiaggregatory effect on ADP-stimulated hPRP according to the Born method using single cuvettes.

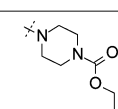
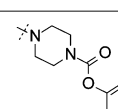
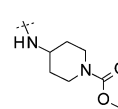
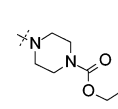
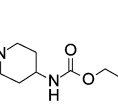
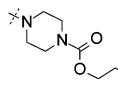
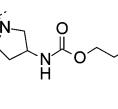
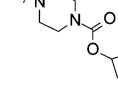
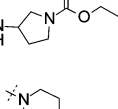
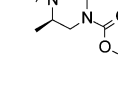
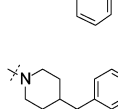
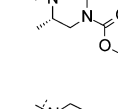
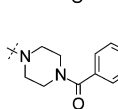
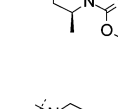
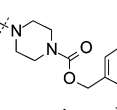
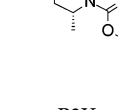
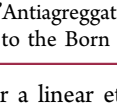
we turned our attention to proline derivatives, which appeared to be closest analogues bearing a similar functionality.

Table 2 shows that even simple primary proline carboxamides like 18a essentially retain the activity as compared to

the initial pyrrolidine derivatives 17h and 17i. However, a remarkable increase in binding affinity and in particular hPRP activity was observed with lipophilic secondary proline amides. A stepwise extension of the lipophilic volume from methyl

Table 3. Binding and hPRP Activity of Variations around the Piperazine Ethyl Carbamate



Compd	R	K_i (P2Y ₁₂) ^a (nM)	IC ₅₀ (hPRP) ^{b,c} (μ M)	Compd	R	K_i (P2Y ₁₂) ^a (nM)	IC ₅₀ (hPRP) ^{b,c} (μ M)
18i		7.3	0.025 (0.009)	19i		71	1.08
19a		>5000	>5.00	19j		3.1	0.021 (0.030)
19b		22	0.555 (0.120)	19k		0.8	0.019 (0.013)
19c		82	1.88	19l		5.0	0.014 (0.042)
19d		193	>5.00	19m		7.7	0.072 (0.021)
19e		30	0.790	19n		54	0.430
19f		40	1.33	19o		80	1.51
19g		130	1.23	19p		51	0.335
19h		5.7	0.124				

^aP2Y₁₂ binding assay using cell membranes from CHO cells with recombinant expression of human P2Y₁₂ receptors employing [³³P]2-MeS-ADP as the radioligand. ^bAntiaggregatory effect on ADP-stimulated hPRP using a 96-well format. ^cIn parentheses: Antiaggregatory effect on ADP-stimulated hPRP according to the Born method using single cuvettes.

amide **18b** over a linear ethyl amide **18c** to a *n*-propyl amide **18d** [IC₅₀ (hPRP): 0.058 μ M] strongly increased the activity. Successive branching of the terminal lipophilic amide from the isopropyl amide **18e** to the spherical *tert*-butyl amide **18f** further enhanced the activity [IC₅₀ (hPRP): 0.040 and 0.017 μ M]. Notably, the cyclopropyl amide **18g** [IC₅₀ (hPRP): 0.013 μ M] was even more potent as compared to the corresponding isosteric acyclic isopropyl amide **18e**. Interestingly, the (*R*)-enantiomer **18h** addressing the opposite trajectory of (*S*)-enantiomer **18g** showed a more than 10-fold drop of binding affinity as compared to **18g**, suggesting a highly specific hydrophobic interaction of **18g** with the receptor. Further

extension of the ring size from a cyclopropyl amide (**18g**) to a cyclobutyl amide (**18i**) or cyclopentyl amide (**18j**) unveiled one of the most potent substitution patterns of the present study, displaying optimal binding affinity and hPRP activity in the nanomolar range [K_i (P2Y₁₂): 7.3 and 20 nM; IC₅₀ (hPRP): 0.025 and 0.013 μ M]. This very subtle interaction is further illustrated by the compounds **18k**–**18m**. Small variations from the optimal presentation of the cyclobutyl moiety like a proline *N*-methyl-cyclobutyl amide **18k**, a methylene-linker extension in **18l**, or the ring-contracted proline analogue, azetidine **18m**, resulted in moderate loss of binding affinity and a moderate to significant drop of hPRP activity. Stronger deviations from the

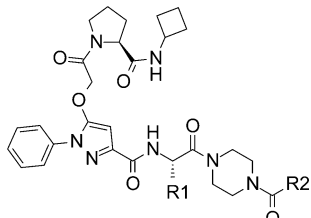
optimal trajectorial angle presenting the cyclobutyl carboxamide moiety as in compounds **18n** or **18o** turned out to be deleterious for the activity [K_i (P2Y₁₂): 238 and 613 nM; IC₅₀ (hPRP): 3.13 and 2.94 μM]. Next, we explored compounds bearing a cyclic amide variation of increasing ring size. Again, even small, incremental changes from the moderately active pyrrolidine carboxamide **18p** to the piperidine carboxamide **18q** were sufficient to obtain an acceptable binding affinity and potency in hPRP [K_i (P2Y₁₂): 219 vs 56 nM; IC₅₀ (hPRP): 0.60 vs 0.070 μM]. The attempted bioisosteric replacement of the carboxamide group with an imidazole moiety resulted in the reasonably active compound **18r**. Notably, the profound impact of the lipophilic interaction with the receptor at this region was also demonstrated when the entire alkyl carboxamide was omitted and replaced by a phenyl ring. Despite the relatively large structural change, this compound **18s** displayed an unexpectedly high binding affinity and hPRP activity as compared to several other more conservative variations of the proline cyclobutyl amide motif [K_i (P2Y₁₂): 33 nM; IC₅₀ (hPRP): 0.29 μM].

These results indicate that the 5-position of the pyrazole ring directs the substituent to a lipophilic pocket, which exhibits a steric confinement, as illustrated by the significant drop of activity, if the ideal geometry is violated. A more concise structure-based rationalization of the observed SAR is provided in the section Development of 3D QSAR Models.

The results in Table 2 established the structural requirements for the decoration of the 5-position of the phenylpyrazole with the *N*-acetyl-(*S*)-proline cyclobutyl amide residue as the optimal substituent. We next turned our attention toward a potential optimization of the piperazine carbamate portion of our preliminary lead compound (Table 3). Our docking hypothesis (Figure 1) proposed that this substituent points to the extracellular site of the receptor and establishes interactions with residues from the ECs. Because we considered the accuracy of our protein model in this region to be very low, a reliable structure-based rationalization of the piperazine carbamate SAR was not feasible. Nevertheless, the preference for lipophilic residues of a certain length (e.g., butyl substituents) was captured by the steric fields of the CoMSIA model (see Figure 3). Introducing a 4-amino piperidine group as a piperazine homologue resulted in the considerably less active compound **19a** (Table 3). Interestingly, **19b** incorporating the inverse 4-amino piperidine spacer exhibited a higher binding affinity to the receptor and had a much higher activity in hPRP than **19a** [K_i (P2Y₁₂): 22 vs >5000 nM; IC₅₀ (hPRP): 0.055 vs >5.0 μM]. The same trend was also observed for the related analogues, the corresponding 3-amino pyrrolidine compounds **19c** and **19d**, which confirmed that a C-terminal attachment of the glutamic acid to a secondary amine is crucial for high receptor affinity. Any effort to replace the alkyl carbamate unit by more rigid *N*-aryl piperazines like in **19e** or *N*-acyl piperazines like in **19g** was unsuccessful and did not lead to compounds of higher binding affinity or hPRP activity. In contrast, very conservative variations of the alkyl carbamate moiety turned out to be most effective. Simple alkyl extension from ethyl (**18i**) to *n*-propyl (**19j**) and *n*-butyl (**19k**) provided derivatives that showed the highest binding affinities and an extraordinarily good hPRP activity [K_i (P2Y₁₂): 3.1 and 0.8 nM; IC₅₀ (hPRP): 0.021 and 0.019 μM]. An equal potency was found for the cyclobutyl derivative **19l** [K_i (P2Y₁₂): 5.0 nM; IC₅₀ (hPRP): 0.014 μM]. In an attempt to rigidify and restrict the conformational flexibility of the piperazine spacer, the

corresponding 2- or 3-methyl-substituted piperazines **19m–p** were investigated. Interestingly, a pronounced influence of the position and absolute configuration of the methyl group was observed. Among the variations **19m** to **19p**, only the (3*R*)-configured stereoisomer **19m** was able to restore the activity of the nonsubstituted piperazine derivative **18i** in the binding and hPRP assay. All other variations were less active. This result is indicative for the considerable spatial restrictions and conformational preferences for the receptor–ligand interaction.

Previous studies^{11a,c,16,18} suggested an indispensable role of the γ -carboxylic acid moiety of the central glutamic acid for binding affinity by a strong putative salt bridge interaction with Lys7.35 and Arg6.55 at the ADP binding pocket (see also Figure 2). Despite these putative prerequisites, we hypothesized that the remarkably strong receptor interaction of the *N*-acetyl-(*S*)-proline cyclobutyl amide-substituted pyrazolone backbone would allow us to vary the central amino acid region without a serious loss of activity. Table 4 shows the set of variations made to probe the significance of the side chain of the glutamic acid linker and to evaluate the spatial and electrostatic environment. Examination of compounds bearing polar amino acid side chains like sulfonamide **20a** or **20b** did not reveal any superior motif than the glutamic acid moiety in **18i**. None of these variations showed hPRP IC₅₀ values better than 100 nM. Nonetheless, the detected binding affinities around 100 nM for those ligands indicated that there were no severe unfavorable interactions present. Consequently, when the carboxylic acid portion in compounds **18i** and **19k** was replaced by the nonclassical bioisostere tetrazole, equally potent compounds **20c** and **20d** were obtained [K_i (P2Y₁₂): 5.0 and 1.5 nM; IC₅₀ (hPRP): 0.040 and 0.050 μM]. In agreement with our docking hypothesis, introduction of a basic ethyl amine side chain **20e** led to a significant drop of activity, which could be partially recovered by acetylation (**20f**), suggesting that the amino acid side chain is accommodated in a positively charged environment of the receptor. Notably, the simple noncharged C2 serine homologue **20g** turned out to be very active [K_i (P2Y₁₂): 23 nM; IC₅₀ (hPRP): 0.210 μM]. Further chain elongation led to the corresponding C3 serine homologue **20h**, which exhibited an even higher binding affinity and a hPRP activity in the low nanomolar range [K_i (P2Y₁₂): 6.5 nM; IC₅₀ (hPRP): 0.092 μM]. However, commencing spatial restrictions became evident with the corresponding longer hydroxyl derivative **20i**, which was found to be inferior in terms of both binding affinity and hPRP activity. Deletion of any polarity by introducing linear and branched lipophilic amino acids of different length and extension (**20j–m**) showed in general lower binding affinities and much lower hPRP activities, supporting the hypothesis that there are no favorable hydrophobic contacts at this site of the receptor binding pocket and that competing plasma protein binding due to the increased lipophilicity is likely. Unexpectedly, replacement of alanine (**20m**) by glycine (**20n**) led to a more than 20-fold increase in hPRP activity through sole omission of a single methyl group [K_i (P2Y₁₂): 111 vs 107 nM; IC₅₀ (hPRP): 0.090 vs 2.21 μM]. The corresponding *n*-butyl carbamate **20o** was found to be even more potent in the binding assay and in the hPRP assay, closely reaching the potency of the analogues bearing the glutamic acid linker [K_i (P2Y₁₂): 7.7 nM; IC₅₀ (hPRP): 0.030 μM]. One might hypothesize that in the absence of the glutamic acid or any other side chain, the interaction with the basic residues is established via one or more water molecules. However, this result was highly unexpected as in related series described by

Table 4. Binding and hPRP Activity of Compounds with Variations around the Central Amino Acid Moiety


Compds	R1	R2	K_i (P2Y ₁₂) ^a (nM)	IC ₅₀ (hPRP) ^{b,c} (μ M)
20a		OEt	48	1.200
20b		OEt	23	0.130
20c		OEt	5.0	0.040 (0.069)
20d		OBu	1.5	0.050 (0.079)
20e		OEt	180	3.77
20f		OEt	42	0.675
20g		OEt	23	0.210 (0.120)
20h		OBu	6.5	0.092 (0.070)
20i		OEt	202	2.400
20j		OEt	172	3.61
20k		OEt	207	>5.0
20l		OEt	183	1.90
20m		OEt	111	2.21
20n		OEt	107	0.090 (0.100)
20o		OBu	7.7	0.030 (0.046)

^aP2Y₁₂ binding assay using cell membranes from CHO cells with recombinant expression of human P2Y₁₂ receptors employing [³³P]-2-MeS-ADP as the radioligand. ^bAntiaggregatory effect on ADP-stimulated hPRP using a 96-well format. ^cIn parentheses: Antiaggregatory effect on ADP-stimulated hPRP according to the Born method using single cuvettes.

others,^{11a,c} the corresponding glycine analogues were found to be inactive in the hPRP assay. Therefore, it has to be anticipated that the strong impact of the cyclic amides at the 5-position of the pyrazole on the hPRP activity apparently outbalances the absence of the carboxyl group of the glutamic acid moiety, which usually is required to obtain good activities in both binding and hPRP assays.

Selected compounds were further evaluated to elucidate the origin of the observed very high inhibitory activity in the hPRP assay as compared to the initial lead 4 (Table 5). To estimate

Table 5. Activity and Selectivity Data of Selected Compounds Using P2Y₁ Cell Membranes and IPs Stimulated with Different Agonists

	compds			
	4	18i	20n	20o
K_i (P2Y ₁₂) ^a	139 nM	7.3 nM	107 nM	7.7 nM
K_i (P2Y ₁) ^b	>20 μ M	>20 μ M	ND	>20 μ M
IC ₅₀ (IP, ADP) ^c	0.701 μ M	0.007 μ M	0.099 μ M	0.022 μ M
IC ₅₀ (hPRP, ADP) ^d	2.93 μ M	0.009 μ M	0.100 μ M	0.046 μ M
IC ₅₀ (IP, col) ^e	>2 μ M	>2 μ M	>2 μ M	>2 μ M
IC ₅₀ (IP, thr) ^f	>2 μ M	>2 μ M	>2 μ M	>2 μ M

^aP2Y₁₂ binding assay using cell membranes from CHO cells with recombinant expression of human P2Y₁₂ receptors employing [³³P]-2-MeS-ADP as the radioligand. ^bP2Y₁ binding assay using cell membranes from CHO cells with recombinant expression of human P2Y₁ receptors employing [³³P]-2-MeS-ADP as the radioligand. ^cAntiaggregatory effect on ADP-stimulated human IPs according to the Born method using single cuvettes. ^dAntiaggregatory effect on ADP-stimulated hPRP according to the Born method using single cuvettes. ^eAntiaggregatory effect on collagen (col)-stimulated human IP according to the Born method using single cuvettes. ^fAntiaggregatory effect on thrombin (thr)-stimulated human IP according to the Born method using single cuvettes.

the contribution of a reduced association of the compounds to plasma proteins, the antiaggregatory activity with isolated platelets (IPs) preparations was determined to avoid additional blood components interfering with the inhibitory effects. As expected from the binding affinity and hPRP data, lead 4 was also the least active compound on IPs. Moreover, a comparison of the respective activity in hPRP reveals that lead compound 4 exhibits the highest loss of antiaggregatory activity in hPRP with a 4-fold shift in the presence of plasma proteins [IC₅₀ (IP): 0.701 μ M vs IC₅₀ (hPRP): 2.93 μ M]. In contrast, the compounds 18i, 20n, and 20o, bearing the *N*-acetyl-(*S*)-proline cyclobutyl amide moiety, showed only a moderate shift in activity in hPRP as compared to IP, thus indicating that the association to plasma proteins does not impair the antiaggregatory activity to a significant extent. To exclude that the observed strong antagonistic action of these compounds originates from the interference of the ligands with other activation pathways, IPs were stimulated using Col and Thr as agonists in the presence of the 4, 18i, 20n, and 20o. Neither the Col- nor the Thr-stimulated aggregation was affected at relevant concentrations by 4, 18i, 20n, and 20o.^{9,19} In addition, these compounds were highly selective versus the P2Y₁ receptor, thus excluding any synergistic interaction and contribution of this receptor. These results clearly indicate that the observed strong inhibition of the ADP-mediated platelet aggregation in hPRP is due to the specific antagonistic action on the P2Y₁₂ receptor. Moreover, apart from the high functional activity shown in IP, the reduced plasma protein

binding appears to contribute to the observed high antagonistic activity in hPRP.

The potential for the further development of these compounds was underscored by the evaluation of the antiaggregatory activity in an ex-vivo dog model.^{9,20} For example, when **20o** was orally administered with 10 mg/kg a sustained antiaggregatory effect with 73% inhibition after 24 h [whole blood platelet aggregation (impedance), 2.5 μ M ADP, area under curve (AUC mean)] was observed.

4. DEVELOPMENT OF 3D QSAR MODELS

Because the binding hypotheses provided in this publication were based on docking modes into homology models and not on high-resolution crystal structures, we generated multiple ligand alignments for the establishment of 3D QSAR [comparative molecular field analysis (CoMFA) and CoMSIA] models to reveal essential features for activity. Starting with the docking mode of **4** (Figure 2) as a reference, all remaining compounds were consistently aligned with our multiple ligand alignment approach Multiple Alignments by ROCS-based Similarity (MARS).²¹ On the basis of this alignment, statistically good CoMFA ($q_{\text{LOO}}^2 = 0.60$, $q_{\text{LNO}}^2 = 0.59$ for four partial least-squares components) and CoMSIA ($q_{\text{LOO}}^2 = 0.63$, $q_{\text{LNO}}^2 = 0.62$ for four partial least-squares components) models were obtained. The steric and electrostatic std*coeff fields of the CoMSIA model are shown in Figure 3 with **4** [K_i (P2Y₁₂): 139 nM]. Green contours indicate regions where steric bulk is favorable for P2Y₁₂ activity, whereas yellow contours highlight regions where substituents are detrimental for activity.

Because the reference conformation for the multiple ligand alignment was based on a docking hypothesis in the P2Y₁₂ receptor, the contour fields can be analyzed in the context of the binding site (model) environment. Indeed, the maps are consistent with steric and electrostatic requirements of the modeled P2Y₁₂ binding site. For example, the carboxy group of the central glutamic acid of the initial lead **4** is located close to a region (indicated by a red contour) where negatively charged substituents are favorable for activity due to electrostatic interactions to the cationic amino acids Arg6.55 and Lys7.35. Figure 3 panels a–d illustrate the SAR of the substituents at the 5-position of the pyrazole moiety. The beneficial effect of lipophilic substituents at the 5-position is visualized in Figure 3b,c by the steric fields (indicated by a green contour). For example, the propyl side chain of **18d** [K_i (P2Y₁₂): 66 nM] is located in a green contour field, where additional steric bulk is favorable for affinity. This is in contrast to the methyl substituent of **18b**, which shows a considerably lower activity [K_i (P2Y₁₂): 536 nM]. Figure 3d explains the configurational dependence of the activity for the proline stereoisomers **18g** and **18h** (Table 2). Whereas the (*S*)-configured stereoisomer **18g** [K_i (P2Y₁₂): 105 nM] shows an optimal interaction with the modeled binding site, the (*R*)-configured stereoisomer **18h** [K_i (P2Y₁₂): 958 nM] clashes with the surrounding protein residues, resulting in a less favorable overall fit of the molecule in the receptor binding site.

5. CONCLUSION

We have developed a series of highly active P2Y₁₂ antagonists based on a phenylpyrazolone scaffold. Investigation of the structural requirements at three different regions generated a set of structural diverse P2Y₁₂ antagonists. Notably, noncharged

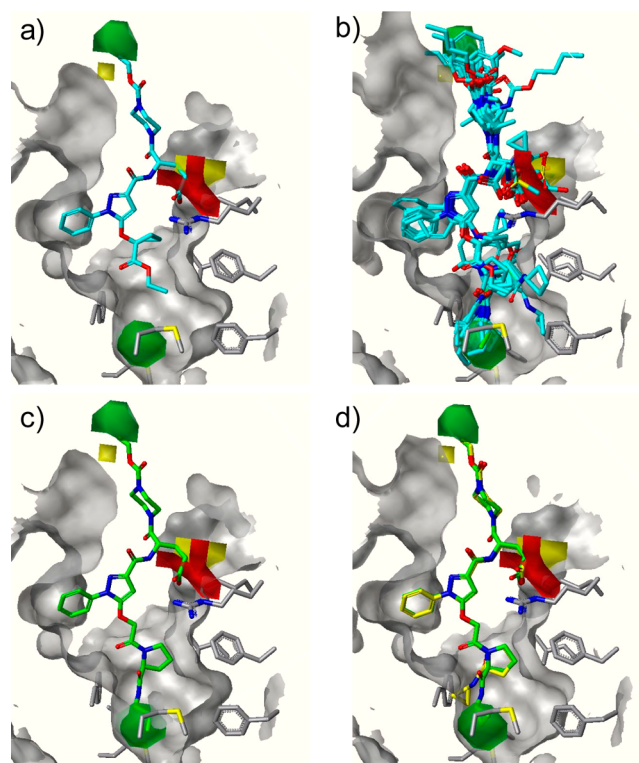


Figure 3. (a) Shows steric and electrostatic std*coeff contour maps from the CoMSIA model with our initial lead compound **4** [K_i (P2Y₁₂), 139 nM]: Green contours refer to regions where additional steric bulk is favorable for affinity, while yellow contours indicate disfavored areas. Red contours indicate regions where negatively charged substituents are favorable. (b) The same as panel a with all 63 compounds aligned. (c) The same as panel a with **18d** [K_i (P2Y₁₂), 66 nM]. (d) The same as panel a with **18g** [molecule shown in green; K_i (P2Y₁₂), 105 nM] and **18h** [yellow; K_i (P2Y₁₂), 958 nM].

residues attached to the 5-*O*-position of the pyrazolone like the *N*-acetyl-(*S*)-proline cyclobutyl amide group accumulated strong evidence that these moieties address a distinct binding pocket of the receptor. Addressing this binding pocket resulted in not only an increase in binding affinity but also a dramatic increase of functional hPRP activity, a recognized parameter for the antithrombotic activity in the clinic, up to the low nanomolar range. Surprisingly, revisiting the structural requirements of the piperazinyl ethyl carbamate and the central glutamic acid moiety revealed that the charged glutamate residue could be replaced by a glycine. This was highly unexpected, as the glutamic residue had been previously considered to form an indispensable strong interaction with the basic residues Arg6.55 and Lys7.35 of the P2Y₁₂ receptor. Further investigations using IPs and other agonists revealed a reduced association to plasma proteins of these compounds as compared to the initial lead **4** and excluded the interference of the antagonists with other significant activation pathways. These results underscore the key role played by the high affinity *N*-acetyl-(*S*)-proline cyclobutyl amide ligand moiety, in determining not only the high binding affinity but also the strong functional hPRP activity. Exploiting this behavior may potentially allow the generation of other highly potent P2Y₁₂ antagonists by using other *N*-acetyl-(*S*)-proline cyclobutyl amide ligand–scaffold combinations.

6. EXPERIMENTAL SECTION

6.1. Chemistry. Solvents and other reagents were used as received without further purification. Normal phase column chromatography was carried out on Merck silica gel 60 (230–400 mesh). Reversed phase high-pressure chromatography was conducted on an Agilent 1100 instrument using an Agilent Prep. C18 column (10 μ m, 30 mm \times 250 mm). Thin-layer chromatography (TLC) was carried out on TLC aluminum sheets with silica gel 60F254 from Merck. Varying ratios of acetonitrile and 0.1% trifluoroacetic acid in water were used as solvent systems. NMR spectra were recorded in CD₃OD, CDCl₃, or DMSO-*d*₆ either on a Bruker DRX 400 or a Bruker FN-ARX 500. Chemical shifts are reported as δ values from an internal tetramethylsilane standard. All final compounds were purified by normal phase or reversed phase chromatography. Purity and characterization of compounds were established by a combination of analytical HPLC, LC-MS, and NMR analytical techniques. All tested compounds were found to be >95% pure by analytical HPLC and LC-MS analysis.

LC-MS analyses were performed with an Agilent HPLC Series 1100. The following HPLC methods were used to obtain the reported retention times. Method a: YMC Jsphere column 33 mm \times 2 mm; 4 μ m; flow rate, 1.0 mL/min. Gradient: water + 0.05% trifluoroacetic acid:acetonitrile + 0.05% trifluoroacetic acid: 98 (1 min) to 95:5 (5.0 min) to 95:5 (6.25 min); Waters LCT-MUX, ESI+ mode. Method b: YMC Jsphere column 33 mm \times 2 mm; 4 μ m; flow rate, 1.0 mL/min. Gradient: water + 0.05% trifluoroacetic acid:acetonitrile + 0.05% trifluoroacetic acid 95:5 (0 min) to 5:95 (3.7 min); Waters LCT-MUX, ESI+ mode. Method c: Waters XBridge C18 column 4.6 mm \times 50 mm; 2.5 μ m; flow rate, 1.3 mL/min. Gradient: water + 0.1% formic acid:acetonitrile + 0.08% formic acid 97:3 (0 min) to 40:60 (3.5 min) to 2:98 (4 min) to 2:98 (5 min) to 97:3 (5.2 min) to 97:3 (6.5 min); Waters Quattro Ultima, ESI+ mode. Method d: Waters XBridge C18 column 4.6 mm \times 50 mm; 2.5 μ m; flow rate, 1.3 mL/min. Gradient: water + 0.05% trifluoroacetic acid:acetonitrile + 0.05% trifluoroacetic acid 95:5 (0 min) to 95:5 (0.3 min) to 5:95 (3.5 min) to 5:95 (4 min); Waters LCT, ESI+ mode. Method e: YMC Jsphere column 33 mm \times 2 mm; 4 μ m; flow rate, 1.3 mL/min. Gradient: water + 0.05% trifluoroacetic acid:acetonitrile + 0.05% trifluoroacetic acid 95:5 (0 min) to 5:95 (2.5 min) to 95:5 (3.2 min); Waters LCT, ESI+ mode. Method f: YMC Jsphere column 33 mm \times 2 mm; 4 μ m; flow rate, 1.0 mL/min. Gradient: water + 0.05% trifluoroacetic acid:AcN + 0.05% trifluoroacetic acid 95:5 (0 min) to 5:95 (3.7 min); Waters LCT-MUX, ESI+ mode. Method g: YMC Jsphere column 33 mm \times 2 mm; 4 μ m; flow rate, 1.3 mL/min. Gradient: water + 0.05% formic acid:acetonitrile + 0.05% formic acid 95:5 (0 min) to 5:95 (0.5 min) to 5:95 (3.5 min) to 5:95 (4 min); Waters LCT, ESI+ mode. Method h: YMC Jsphere column 33 mm \times 2 mm; 4 μ m; flow rate, 1.3 mL/min. Gradient: water + 0.05% formic acid:acetonitrile + 0.05% formic acid 95:5 (0 min) to 5:95 (2.5 min); Waters Quattro Ultima, ESI+ mode. Method i: YMC Jsphere column 33 mm \times 2 mm; 4 μ m; flow rate, 1.3 mL/min. Gradient: water + 0.1% formic acid:acetonitrile + 0.08% formic acid 95:5 (0 min) to 5:95 (2.5 min); Waters Quattro Ultima, ESI+ mode. Method j: YMC Jsphere column 20 mm \times 2 mm; 4 μ m; flow rate, 1.0 mL/min. Gradient: water + 0.05% trifluoroacetic acid:acetonitrile + 0.05% trifluoroacetic acid 94:6 (0 min) to 5:95 (2.4 min) to 94:6 (2.45 min); Agilent series 1100 MSD, ESI+ mode.

6.1.1. 4-((S)-2-Amino-4-tert-butoxycarbonyl-butyl)-piperazine-1-carboxylic Acid Ethyl Ester (7). **6.1.1.1. 4-((S)-2-Benzylloxycarbonylamino-4-tert-butoxycarbonyl-butyl)-piperazine-1-carboxylic Acid Ethyl Ester.** To a solution of (S)-2-benzylloxycarbonylamino-pentanedioic acid 5-tert-butyl ester (5) (15.0 g, 44.5 mmol) in DMF (75 mL) were added 1-ethoxycarbonylpiperazine (6) (6.9 mL, 44.5 mmol), N-ethylmorpholine (22.6 mL, 177.8 mmol), and TOTU (14.6 g, 44.5 mmol). After it was stirred for 12 h, the solution was diluted with ethyl acetate and subsequently washed with aqueous LiCl (4% w/w) and saturated aqueous NaHCO₃. The crude product (20.9 g, 99%) obtained after evaporation of the solvent was directly subjected to the subsequent deprotection reaction without further purification. ¹H NMR (DMSO-*d*₆): δ 7.52 (d, *J* = 8.3 Hz, 1H), 7.34 (m, 5H), 5.04 (d, *J* = 12.6 Hz, 1H), 4.99 (d, *J* = 12.6 Hz, 1H), 4.47 (m, 1H), 4.06 (q, *J* =

7.4 Hz, 2H), 3.52 (m, 4H), 3.39 (m, 4H), 2.27 (m, 2H), 1.80 (m, 1H), 1.67 (m, 1H), 1.39 (s, 9H), 1.19 (t, *J* = 7.4 Hz, 3H). *t*_R (method j): 1.52 min. MS (ES) *m/z*: 478.3 (MH⁺).

6.1.1.2. 4-((S)-2-Amino-4-tert-butoxycarbonyl-butyl)-piperazine-1-carboxylic Acid Ethyl Ester (7). To a solution of 4-((S)-2-benzylloxycarbonylamino-4-tert-butoxycarbonyl-butyl)-piperazine-1-carboxylic acid ethyl ester (20.9 g, 43.9 mmol) in ethanol (120 mL) was added Pd/C (2.0 g, 10% w/w), and the suspension was stirred under an atmosphere of hydrogen (3 bar) for 12 h. The reaction mixture was filtrated over a plug of Celite, washed with ethanol, and concentrated to give the pure product 7 (13.6 g, 89%) as a colorless oil, which was not further purified. ¹H NMR (DMSO-*d*₆): δ 4.06 (q, *J* = 7.4 Hz, 2H), 3.57 (m, 1H), 3.49 (m, 4H), 3.37 (m, 4H), 2.30 (m, 2H), 1.65 (m, 2H), 1.39 (s, 9H), 1.19 (t, *J* = 7.4 Hz, 3H). *t*_R (method j): 0.82 min. MS (ES) *m/z*: 344.3 (MH⁺).

6.1.2. 5-Carboxymethoxy-1-phenyl-1H-pyrazole-3-carboxylic Acid Ethyl Ester (9). **6.1.2.1. 5-Benzylloxycarbonylmethoxy-1-phenyl-1H-pyrazole-3-carboxylic Acid Ethyl Ester.** To a solution of 5-hydroxy-1-phenyl-1H-pyrazole-3-carboxylic acid ethyl ester (8) (10.0 g, 43.1 mmol) in DMF (100 mL) were added benzyl bromoacetate (7.1 mL, 43.1 mmol) and cesium carbonate (24.0 g, 86.1 mmol). After it was stirred for 16 h at room temperature, the suspension was filtered, washed with DMF, and concentrated. The residue was taken up with ethyl acetate and extracted with aqueous LiCl (4% w/w). Evaporation of the solvent yielded the crude product as a yellow oil (15.5 g, 95%), which was used in the subsequent debenzoylation reaction. *t*_R (method j): 1.64 min. MS (ES) *m/z*: 381.2 (MH⁺).

6.1.2.2. 5-Carboxymethoxy-1-phenyl-1H-pyrazole-3-carboxylic Acid Ethyl Ester (9). To a solution of 5-benzylloxycarbonylmethoxy-1-phenyl-1H-pyrazole-3-carboxylic acid ethyl ester (15.5 g, 40.8 mmol) in ethyl acetate (100 mL) was added Pd/C (1 g, 10%), and the resulting suspension stirred under an atmosphere of hydrogen (3 bar) for 5 h. The reaction mixture was filtered over a plug of Celite and washed with ethyl acetate and methanol to give the crude product 9 as colorless platelets (11.5 g, 98%) after evaporation of the solvents. ¹H NMR (DMSO-*d*₆): δ 13.28 (s br, 1H), 7.74 (d, *J* = 7.9 Hz, 2H), 7.54 (t, *J* = 7.9 Hz, 2H), 7.42 (t, *J* = 7.9 Hz, 1H), 6.42 (s, 1H), 4.93 (s, 2H), 4.29 (q, *J* = 7.0 Hz, 2H), 1.30 (t, *J* = 7.0 Hz, 3H). *t*_R (method j): 1.11 min. MS (ES) *m/z*: 291.2 (MH⁺).

6.1.3. Preparation of 5-[2-((S)-2-cyclobutylcarbamoyl-pyrrolidin-1-yl)-2-oxo-ethoxy]-1-phenyl-1H-pyrazole-3-carboxylic Acid (10). **6.1.3.1. 5-[2-((S)-2-Benzylloxycarbonyl-pyrrolidin-1-yl)-2-oxo-ethoxy]-1-phenyl-1H-pyrazole-3-carboxylic Acid Ethyl Ester.** To a solution of 5-carboxymethoxy-1-phenyl-1H-pyrazole-3-carboxylic acid ethyl ester (9) (9.5 g, 32.8 mmol) in DMF (100 mL) were added HOBt (5.0 g, 32.8 mmol), EDC (6.3 g, 32.8 mmol), and DIPEA (10.9 mL, 65.7 mmol). After 5 min, L-proline benzyl ester hydrochloride (7.9 g, 32.8 mmol) was added, and the resulting solution was stirred for 16 h. The reaction mixture was concentrated, dissolved in dichloromethane, and extracted with aqueous LiCl (4% w/w) and saturated NaHCO₃. The crude product obtained after evaporation of the solvent was purified by flash chromatography on silica using ethyl acetate/heptane 1:1 as an eluent to give the product as colorless foam (13.2 g, 84%). *t*_R (method j): 1.55 min. MS (ES) *m/z*: 478.3 (MH⁺).

6.1.3.2. 5-[2-((S)-2-Carboxy-pyrrolidin-1-yl)-2-oxo-ethoxy]-1-phenyl-1H-pyrazole-3-carboxylic Acid Ethyl Ester. To a solution of 5-[2-((S)-2-benzylloxycarbonyl-pyrrolidin-1-yl)-2-oxo-ethoxy]-1-phenyl-1H-pyrazole-3-carboxylic acid ethyl ester (13.2 g, 27.6 mmol) in ethyl acetate (100 mL) was added Pd/C (1 g, 10%), and the resulting suspension was stirred under an atmosphere of hydrogen (3 bar) for 6 h. The reaction mixture was filtered over a plug of Celite and washed with ethanol to give the crude product as colorless foam (8.9 g, 70%) after evaporation of the solvents. ¹H NMR (DMSO-*d*₆): δ 12.61 (s br, 1H), 7.83 (d, *J* = 8.4 Hz, 2H), 7.57 (t, *J* = 7.8 Hz, 2H), 7.45 (t, *J* = 7.8 Hz, 1H), 6.48 (s, appears as 2 rotamers, 1H), 5.12 (s, 2H), 4.32 (m, 3H), 3.55 (m, 2H), 2.15 (m, 1H), 1.89 (m, 3H), 1.28 (t, *J* = 7.0 Hz, 3H). *t*_R (method j): 1.10 min. MS (ES) *m/z*: 388.2 (MH⁺).

6.1.3.3. 5-[2-((S)-2-Cyclobutylcarbamoyl-pyrrolidin-1-yl)-2-oxo-ethoxy]-1-phenyl-1H-pyrazole-3-carboxylic Acid Ethyl Ester. To a solution of 5-[2-((S)-2-carboxy-pyrrolidin-1-yl)-2-oxo-ethoxy]-1-phenyl-

nyl-1H-pyrazole-3-carboxylic acid ethyl ester 84.5 g, 11.6 mmol) in DMF (105 mL) were added HATU (4.4 g, 11.6 mmol) and DIPEA (1.9 mL, 11.6 mmol). After 10 min, cyclobutylamine (1.0 mL, 11.6 mmol) was added, and after 30 min, the reaction mixture was concentrated. The residue was taken up in dichloromethane and extracted with aqueous LiCl (4% w/w), aqueous HCl (0.1 M), and saturated NaHCO₃. The crude product obtained after evaporation of the solvent was purified by flash chromatography on silica using ethyl acetate/heptane 4:1 as the eluent to give the title compound as a colorless oil (3.2 g, 62%). *t_R* (method j): 1.26 min. MS (ES) *m/z*: 441.3 (MH⁺).

6.1.3.4. 5-[2-((S)-2-Cyclobutylcarbamoyl-pyrrolidin-1-yl)-2-oxo-ethoxy]-1-phenyl-1H-pyrazole-3-carboxylic Acid (10). To a solution of 5-[2-((S)-2-cyclobutylcarbamoyl-pyrrolidin-1-yl)-2-oxo-ethoxy]-1-phenyl-1H-pyrazole-3-carboxylic acid ethyl ester (3.2 g, 7.2 mmol) in THF (40 mL) and water (5 mL) was added NaOH (340 mg, 8.5 mmol) portionwise at 0 °C. After 4 h, the solution was neutralized with Amberlite IR-120 ion-exchange resin, filtered, and washed with methanol. After evaporation of the solvents, the product **10** was obtained as a yellow gum (3.7 g, 77%). ¹H NMR (DMSO-*d*₆): δ 8.00 (d, appears as 2 rotamers, *J* = 7.5 Hz, 1H), 7.81 (d, *J* = 8.7 Hz, 2H), 7.48 (t, *J* = 8.7 Hz, 2H), 7.33 (t, *J* = 8.7 Hz, 1H), 6.24 (s, appears as 2 rotamers, 1H), 4.99 (s, 2H), 4.22 (dd, *J* = 8.6 Hz, *J* = 3.5 Hz, 1H), 4.14 (m, 1H), 3.56 (m, 1H), 3.47 (m, 1H), 2.20–1.54 (several multiplets, 10H). *t_R* (method j): 1.04 min. MS (ES) *m/z*: 413.2 (MH⁺).

6.1.4. Representative Procedure: Preparation of 4-((S)-4-Carboxy-2-[[5-hydroxy-1-phenyl-1H-pyrazole-3-carbonyl]-amino]-butyryl)-piperazine-1-carboxylic Acid Ethyl Ester (17a). **6.1.4.1. 4-((S)-4-tert-Butoxycarbonyl-2-[[5-hydroxy-1-phenyl-1H-pyrazole-3-carbonyl]-amino]-butyryl)-piperazine-1-carboxylic Acid Ethyl Ester.** To a solution of 1-phenyl-3-carboxy-5-pyrazolone **11** (2 g, 35.2 mmol) and 4-((S)-2-amino-4-tert-butoxycarbonyl-butyl)-piperazine-1-carboxylic acid ethyl ester (**7**) (12.1 g, 35.2 mmol) in DMF (100 mL), HOBt (5.4 g, 35.2 mmol) and EDC (6.7 g, 35.2 mmol) were added, and the reaction mixture was stirred for 12 h at room temperature. Then, the reaction mixture was diluted with ethyl acetate and subsequently extracted with aqueous LiCl (4% w/w), aqueous HCl (0.1 M), and aqueous NaHCO₃. The organic layer was dried over MgSO₄, and the solvent was removed under reduced pressure to yield the product (14.8 g, 80%), which was directly subjected to the subsequent deprotection reaction.

6.1.4.2. 4-((S)-4-Carboxy-2-[[5-hydroxy-1-phenyl-1H-pyrazole-3-carbonyl]-amino]-butyryl)-piperazine-1-carboxylic Acid Ethyl Ester (17a). To a solution of 4-((S)-4-tert-butoxycarbonyl-2-[[5-hydroxy-1-phenyl-1H-pyrazole-3-carbonyl]-amino]-butyryl)-piperazine-1-carboxylic acid ethyl ester (50 mg, 0.09 mmol) in dichloromethane (2 mL), trifluoroacetic acid (0.13 mL) was added. After it was stirred for 4 h, the reaction mixture was concentrated, and the crude product obtained was purified by preparative reversed-phase HPLC, eluting with a gradient of acetonitrile in water (+0.01% trifluoroacetic acid). After lyophilization, the product **17a** (9 mg, 20%) was obtained as a white solid. ¹H NMR (DMSO-*d*₆): δ 12.05 (s br, 1H), 8.09 (d, *J* = 7.8 Hz, 1H), 7.78 (d, *J* = 8.1 Hz, 2H), 7.50 (t, *J* = 7.8 Hz, 2H), 7.35 (t, *J* = 7.1 Hz, 1H), 5.92 (s, 1H), 4.94 (dt, *J* = 4.5 Hz, *J* = 8.8 Hz, 1H), 4.06 (q, *J* = 6.8 Hz, 2H), 3.46 (m, 8H), 2.29 (m, 2H), 1.96 (m, 1H), 1.80 (m, 1H), 1.19 (t, *J* = 6.8 Hz, 3H). *t_R* (method e): 1.39 min. MS (ES) *m/z*: 474.2 (MH⁺).

6.1.5. Representative Procedure: Preparation of 4-((S)-4-Carboxy-2-[[5-(1-ethoxycarbonyl-cyclobutoxy)-1-phenyl-1H-pyrazole-3-carbonyl]-amino]-butyryl)-piperazine-1-carboxylic Acid Ethyl Ester (4). To a solution of 4-((S)-4-tert-butoxycarbonyl-2-[[5-hydroxy-1-phenyl-1H-pyrazole-3-carbonyl]-amino]-butyryl)-piperazine-1-carboxylic acid ethyl ester (1.50 g, 2.8 mmol) in DMF (20 mL), ethyl 1-bromocyclobutanecarboxylate (1.22 g, 5.7 mmol) and cesium carbonate (1.85 g, 5.66 mmol) were added. The reaction mixture was stirred for 2 h at 100 °C, then cooled to room temperature, and diluted with water. The solution was extracted with dichloromethane, and the organic layer was washed with water and dried over MgSO₄. After the solvents were removed under reduced pressure, the residue was purified by flash chromatography on silica using a heptane/ethyl

acetate gradient to give the corresponding O-alkylation product (860 mg, 46%), which was dissolved in dichloromethane (5 mL) and stirred in the presence of trifluoroacetic acid (0.4 mL). After they were stirred for 4 h at room temperature, the solvents were removed under reduced pressure, and the residue was purified by flash chromatography on silica using a dichloromethane/ethanol gradient. After lyophilization, the product **4** (320 mg, 40%) was obtained as a white solid. ¹H NMR (DMSO-*d*₆): δ 8.20 (d, *J* = 8.0 Hz, 1H), 7.76 (d, *J* = 9.0 Hz, 2H), 7.55 (t, *J* = 8.0 Hz, 2H), 7.42 (t, *J* = 7.3 Hz, 1H), 5.84 (s, 1H), 4.93 (m, 1H), 4.17 (q, *J* = 6.9 Hz, 2H), 4.05 (q, *J* = 7.0 Hz, 2H), 3.46 (m, 8H), 2.68 (m, 2H), 2.50 (m, 2H), 2.25 (m, 2H), 1.86 (m, 4H), 1.19 (t, *J* = 6.8 Hz, 3H), 1.12 (t, *J* = 6.8 Hz, 3H). *t_R* (method f): 2.08 min. MS (ES) *m/z*: 600.3 (MH⁺).

6.1.6. Representative Procedure: Preparation of 4-((S)-4-Carboxy-2-[[5-[2-((R)-3-hydroxy-pyrrolidin-1-yl)-2-oxo-ethoxy]-1-phenyl-1H-pyrazole-3-carbonyl]-amino]-butyryl)-piperazine-1-carboxylic Acid Ethyl Ester (17h) via Route 1 (Scheme 2). **6.1.6.1. 4-((S)-2-[[5-Benzyloxycarbonylmethoxy-1-phenyl-1H-pyrazole-3-carbonyl]-amino]-4-tert-butoxycarbonyl-butyl)-piperazine-1-carboxylic Acid Ethyl Ester.** To a solution of 4-((S)-4-tert-butoxycarbonyl-2-[[5-hydroxy-1-phenyl-1H-pyrazole-3-carbonyl]-amino]-butyryl)-piperazine-1-carboxylic acid ethyl ester (14.5 g, 27.3 mmol) in DMF (110 mL) were added benzyl bromoacetate (4.5 mL, 27.3 mmol) and cesium carbonate (17.8 g, 54.7 mmol). After it was stirred at room temperature for 12 h, the solution was reduced to a volume of 50 mL, diluted with ethyl acetate (400 mL), and extracted with aqueous LiCl (4% w/w). The crude product obtained after evaporation of the solvent was purified by flash chromatography on silica eluting with a gradient of *n*-heptane/ethyl acetate to give the title compound as a yellowish amorphous solid (13.2 g, 71%). ¹H NMR (DMSO-*d*₆): δ 8.14 (d, *J* = 8.2 Hz, 1H), 7.77 (d, *J* = 8.0 Hz, 2H), 7.51 (t, *J* = 8.0 Hz, 2H), 7.40 (t, *J* = 8.0 Hz, 1H), 7.36 (m, 5H), 6.42 (s, 1H), 5.21 (s, 2H), 5.11 (s, 2H), 4.95 (m, 1H), 4.05 (m, 3H), 3.58 (m, 4H), 3.42 (m, 4H), 2.28 (m, 2H), 1.96 (m, 1H), 1.81 (m, 1H), 1.37 (s, 9H), 1.19 (t, *J* = 7.0 Hz, 3H). *t_R* (method j): 1.77 min. MS (ES) *m/z*: 678.3 (MH⁺).

6.1.6.2. 4-((S)-4-tert-Butoxycarbonyl-2-[[5-carboxymethoxy-1-phenyl-1H-pyrazole-3-carbonyl]-amino]-butyryl)-piperazine-1-carboxylic Acid Ethyl Ester. To a solution of 4-((S)-2-[[5-benzyloxycarbonylmethoxy-1-phenyl-1H-pyrazole-3-carbonyl]-amino]-4-tert-butoxycarbonyl-butyl)-piperazine-1-carboxylic acid ethyl ester (13.2 g, 19.5 mmol) in ethyl acetate (75 mL) was added under argon Pd/C (1.1 g, 10%), and the suspension was stirred under an atmosphere of hydrogen (3 bar) for 16 h. The suspension was filtered over a plug of Celite and washed with ethyl acetate. The crude product obtained after evaporation of the solvent was dried under vacuo at 40 °C for 24 h to give the title compound as a colorless solid (12.1 g, 100%). ¹H NMR (DMSO-*d*₆): δ 8.14 (d, *J* = 8.2 Hz, 1H), 7.80 (d, *J* = 8.0 Hz, 2H), 7.53 (t, *J* = 8.0 Hz, 2H), 7.41 (t, *J* = 8.0 Hz, 1H), 6.34 (s, 1H), 4.94 (m, 1H), 4.90 (s, 2H), 4.05 (m, 3H), 3.60 (m, 4H), 3.39 (m, 4H), 2.29 (m, 2H), 1.94 (m, 1H), 1.81 (m, 1H), 1.38 (s, 9H), 1.19 (t, *J* = 7.0 Hz, 3H). *t_R* (method j): 1.39 min. MS (ES) *m/z*: 588.3 (MH⁺).

6.1.6.3. 4-((S)-4-Carboxy-2-[[5-[2-((R)-3-hydroxy-pyrrolidin-1-yl)-2-oxo-ethoxy]-1-phenyl-1H-pyrazole-3-carbonyl]-amino]-butyryl)-piperazine-1-carboxylic Acid Ethyl Ester (17h). To a solution of 4-((S)-4-tert-butoxycarbonyl-2-[[5-carboxymethoxy-1-phenyl-1H-pyrazole-3-carbonyl]-amino]-butyryl)-piperazine-1-carboxylic acid ethyl ester (90 mg, 0.15 mmol) in DMF (5 mL) were added DIPEA (54 μL, 0.30 mmol), HOBt (23 mg, 0.15 mmol), and EDC (29 mg, 0.15 mmol). After 20 min, (R)-(-)-3-pyrrolidinyl hydrochloride (19 mg, 0.15 mmol) was added, and the reaction mixture was stirred for 12 h. After dilution with ethyl acetate, the reaction mixture was extracted with aqueous LiCl (4% w/w) and aqueous NaHCO₃. The organic layer was dried over MgSO₄, and the solvent was removed under reduced pressure. The crude product was dissolved in dichloromethane (1.5 mL) and treated with trifluoroacetic acid (127 μL). After they were stirred for 12 h, the solvents were removed under reduced pressure, and the residue was purified by preparative reversed-phase HPLC, eluting with a gradient of acetonitrile in water (+0.01% trifluoroacetic acid). After lyophilization, the product **17h** (45 mg, 49%) was obtained as a white solid. ¹H NMR (DMSO-*d*₆): δ 8.13 (d, *J* = 8.3 Hz, 1H), 7.87 (d, *J* = 8.3 Hz, 2H), 7.52 (t, *J* = 8.3 Hz, 2H), 7.39

(t, $J = 7.4$ Hz, 1H), 6.35 (s, 1H, appears as 2 rotamers), 4.95 (m, 4H), 4.29 (s, 1H, appears as 2 rotamers), 4.05 (q, $J = 6.9$ Hz, 2H), 3.44 (m, 12H), 2.29 (m, 2H), 1.96 (m, 2H), 1.84 (m, 2H), 1.19 (t, $J = 6.8$ Hz, 3H). t_R (method e): 1.22 min. MS (ES) m/z : 501.2 (MH+).

6.1.7. Representative Procedure: Preparation of 4-[(S)-4-Carboxy-2-((S)-[2-((S)-2-methylcarbamoyl-pyrrolidin-1-yl)-2-oxo-ethoxy]-1-phenyl-1H-pyrazole-3-carbonyl)-amino]-butyryl]-piperazine-1-carboxylic Acid Ethyl Ester (18b) via Route 1 (Scheme 2). **6.1.7.1. 4-[(S)-2-((S)-[2-((S)-2-benzoyloxycarbonyl-pyrrolidin-1-yl)-2-oxo-ethoxy]-1-phenyl-1H-pyrazole-3-carbonyl)-amino]-4-tert-butoxycarbonyl-butyl]-piperazine-1-carboxylic Acid Ethyl Ester.** To a solution of 4-[(S)-4-tert-butoxycarbonyl-2-[(S)-carboxymethoxy-1-phenyl-1H-pyrazole-3-carbonyl]-amino]-butyryl]-piperazine-1-carboxylic acid ethyl ester (9.5 g, 16.2 mmol) in DMF (80 mL) were added HOBt (2.5 g, 16.2 mmol), DIPEA (5.7 mL, 32.4 mmol), and L-proline benzyl ester hydrochloride (3.9 g, 16.2 mmol) at 0 °C. At this temperature was added EDC (3.1 g, 16.2 mmol) portionwise, and the suspension was allowed to warm to room temperature over a period of 12 h. The solvent was evaporated, and the residue was dissolved in ethyl acetate and subsequently extracted with aqueous LiCl (4% w/w), aqueous HCl (0.1 M), and aqueous NaHCO₃. The organic layer was dried over MgSO₄, and the solvent was removed under reduced pressure to give the crude product as amorphous solid (11.6 g, 92%). An analytically pure sample could be obtained by purification of an aliquot by preparative HPLC. ¹H NMR (DMSO-*d*₆): δ 8.13 (d, $J = 7.8$ Hz, 1H), 7.84 (d, $J = 7.3$ Hz, 2H), 7.52 (t, $J = 7.3$ Hz, 2H), 7.40 (t, $J = 7.3$ Hz, 1H), 7.33 (m, 5H), 6.38 (s, appears as rotamers, 1H), 5.11 (m, 4H), 4.95 (m, 1H), 4.42 (dd, $J = 9.0$ Hz, $J = 4.3$ Hz, 1H), 4.05 (q, $J = 7.3$ Hz, 2H), 3.56 (m, 10H), 2.33–1.74 (several multiplets, 8H), 1.38 (s, 9H), 1.18 (t, $J = 7.0$ Hz, 3H). t_R (method j): 1.71 min. MS (ES) m/z : 775.3 (MH+).

6.1.7.2. 4-[(S)-4-tert-Butoxycarbonyl-2-((S)-[2-((S)-2-carboxy-pyrrolidin-1-yl)-2-oxo-ethoxy]-1-phenyl-1H-pyrazole-3-carbonyl)-amino]-butyryl]-piperazine-1-carboxylic Acid Ethyl Ester. To a solution of 4-[(S)-2-((S)-[2-((S)-2-benzoyloxycarbonyl-pyrrolidin-1-yl)-2-oxo-ethoxy]-1-phenyl-1H-pyrazole-3-carbonyl)-amino]-4-tert-butoxycarbonyl-butyl]-piperazine-1-carboxylic acid ethyl ester (11.6 g, 14.9 mmol) in ethyl acetate (75 mL) was added under argon Pd/C (1 g, 10%), and the suspension was stirred under an atmosphere of hydrogen (3 bar) for 24 h. The suspension was filtered over a plug of Celite and washed with ethyl acetate. The crude product was obtained after evaporation of the solvent (9.9 g, 89%) and used without further purification. ¹H NMR (DMSO-*d*₆): δ 12.56 (s br, 1H), 8.11 (d, $J = 7.8$ Hz, 1H), 7.85 (d, $J = 7.3$ Hz, 2H), 7.52 (t, $J = 7.3$ Hz, 2H), 7.39 (t, $J = 7.3$ Hz, 1H), 6.37 (s, appears as rotamers, 1H), 5.06 (s, 2H), 4.94 (m, 1H), 4.28 (dd, $J = 9.0$ Hz, $J = 4.1$ Hz, 1H), 4.05 (q, $J = 7.1$ Hz, 2H), 3.57 (m, 5H), 3.42 (m, 5H), 2.31–1.74 (several multiplets, 8H), 1.37 (s, 9H), 1.18 (t, $J = 7.0$ Hz, 3H). t_R (method j): 1.40 min. MS (ES) m/z : 685.3 (MH+).

6.1.7.3. 4-[(S)-4-Carboxy-2-((S)-[2-((S)-2-methylcarbamoyl-pyrrolidin-1-yl)-2-oxo-ethoxy]-1-phenyl-1H-pyrazole-3-carbonyl)-amino]-butyryl]-piperazine-1-carboxylic Acid Ethyl Ester (18b). To a solution of 4-[(S)-4-tert-butoxycarbonyl-2-((S)-[2-((S)-2-carboxy-pyrrolidin-1-yl)-2-oxo-ethoxy]-1-phenyl-1H-pyrazole-3-carbonyl)-amino]-butyryl]-piperazine-1-carboxylic acid ethyl ester (133 mg, 0.19 mmol) in DMF (5 mL) were added DIPEA (80 μ L, 0.49 mmol), HOBt (45 mg, 0.29 mmol), and EDC (56 mg, 0.29 mmol). After 20 min, methylamine hydrochloride (20 mg, 0.29 mmol) was added, and the reaction mixture was stirred for 12 h. After dilution with ethyl acetate, the reaction mixture was extracted with aqueous LiCl (4% w/w) and aqueous NaHCO₃. The organic layer was dried over MgSO₄, and the solvent was removed under reduced pressure. The crude product was dissolved in dichloromethane (4 mL) and treated with trifluoroacetic acid (128 μ L). After this was stirred for 12 h, the solvents were removed under reduced pressure, and the residue was purified by preparative reversed-phase HPLC, eluting with a gradient of acetonitrile in water (+0.01% trifluoroacetic acid). After lyophilization, the product **18b** (46 mg, 37%) was obtained as a white solid. ¹H NMR (DMSO-*d*₆): δ 8.13 (d, $J = 8.4$ Hz, 1H), 7.85 (d, $J = 8.0$ Hz, 2H), 7.76 (m, 1H), 7.53 (t, $J = 7.6$ Hz, 2H), 7.40 (t, $J = 7.4$ Hz, 1H), 6.41 (s, 1H), 5.00 (m, 3H), 4.22 (dd, $J = 8.5$ Hz, $J = 3.2$ Hz,

1H), 4.06 (q, $J = 6.9$ Hz, 2H), 3.51 (m, 10H), 2.55 (d, $J = 4.6$ Hz, 3H), 2.29 (m, 2H), 1.99 (m, 2H), 1.89 (m, 2H), 1.81 (m, 2H), 1.19 (t, $J = 6.8$ Hz, 3H). t_R (method e): 1.25 min. MS (ES) m/z : 642.3 (MH+).

6.1.8. Representative Procedure: Preparation of 4-[(S)-4-Carboxy-2-((S)-[2-((S)-2-cyclobutylcarbamoyl-pyrrolidin-1-yl)-2-oxo-ethoxy]-1-phenyl-1H-pyrazole-3-carbonyl)-amino]-butyrylamino]-piperidine-1-carboxylic Acid Ethyl Ester (19a) via Route 2 (Scheme 2). **6.1.8.1. (S)-2-((S)-[2-((S)-2-Cyclobutylcarbamoyl-pyrrolidin-1-yl)-2-oxo-ethoxy]-1-phenyl-1H-pyrazole-3-carbonyl)-amino)-pentanedioic Acid 5-tert-Butyl Ester 1-Methyl Ester.** To a solution of 5-[[2-((S)-2-cyclobutylcarbamoyl-pyrrolidin-1-yl)-2-oxo-ethoxy]-1-phenyl-1H-pyrazole-3-carboxylic acid (1.1 g, 2.7 mmol) in DMF (20 mL) were added DIPEA (1 mL, 6.1 mmol), HOBt (0.41 g, 2.7 mmol), EDC (0.51 g, 2.7 mmol), and H-Glu(OtBu)-OMe hydrochloride (0.68 g, 2.7 mmol). After it was stirred for 24 h, the solution was concentrated, taken up with dichloromethane, and subsequently extracted with aqueous LiCl (4% w/w), aqueous HCl (0.1 M), and saturated NaHCO₃. The crude product was purified by flash chromatography on silica using an ethyl acetate/heptane 50:50 to 100:0 gradient to give the title compound as a colorless foam (1.88 g, 100%). t_R (method j): 1.55 min. MS (ES) m/z : 612.3 (MH+).

6.1.8.2. (S)-2-((S)-[2-((S)-2-Cyclobutylcarbamoyl-pyrrolidin-1-yl)-2-oxo-ethoxy]-1-phenyl-1H-pyrazole-3-carbonyl)-amino)-pentanedioic Acid 5-tert-Butyl Ester. To a solution of (S)-2-[[2-((S)-2-cyclobutylcarbamoyl-pyrrolidin-1-yl)-2-oxo-ethoxy]-1-phenyl-1H-pyrazole-3-carbonyl)-amino)-pentanedioic acid 5-tert-butyl ester 1-methyl ester (1.84 g, 3.0 mmol) in THF (12 mL) was added LiOH (73 mg, 3.0 mmol) in water (4 mL). After 2 h, the reaction mixture was neutralized with Amberlite IR-120, filtered, and washed with methanol. After evaporation of the solvent, the title compound was obtained as a colorless oil (1.80 g, 100%). ¹H NMR (DMSO-*d*₆): δ 8.24 (d, $J = 7.5$ Hz, 1H), 8.02 (d, $J = 7.5$ Hz, appears as rotamers, 1H), 7.91 (d, $J = 8.3$ Hz, 2H), 7.57 (t, $J = 8.3$ Hz, 2H), 7.43 (t, $J = 8.3$ Hz, 1H), 6.44 (s, 1H, appears as rotamers), 5.09 (s, 2H), 4.44–4.11 (m, 3H), 3.60 (m, 1H), 3.48 (m, 2H), 2.32–1.52 (several multiplets, 14H), 1.37 (s, 9H). t_R (method j): 1.38 min. MS (ES) m/z : 598.2 (MH+).

6.1.8.3. 4-[(S)-4-Carboxy-2-((S)-[2-((S)-2-cyclobutylcarbamoyl-pyrrolidin-1-yl)-2-oxo-ethoxy]-1-phenyl-1H-pyrazole-3-carbonyl)-amino]-butyrylamino]-piperidine-1-carboxylic Acid Ethyl Ester (19a). To a solution of (S)-2-[[2-((S)-2-cyclobutylcarbamoyl-pyrrolidin-1-yl)-2-oxo-ethoxy]-1-phenyl-1H-pyrazole-3-carbonyl)-amino)-pentanedioic acid 5-tert-butyl ester (150 mg, 0.25 mmol) in DMF (7 mL) were added DIPEA (62 μ L, 1.1 mmol), HATU (95 mg, 0.36 mmol), and ethyl 4-amino-1-piperidinecarboxylate (43 mg, 0.25 mmol). After it was stirred for 12 h, the saturated NaHCO₃ solution was added, and the mixture loaded on a chem elut cartridge, the crude product being eluted with dichloromethane. The solution was concentrated to a volume of 1 mL and stirred in the presence of trifluoroacetic acid (190 μ L). After it was stirred for 4 h, the solvents were removed under reduced pressure, and the residue was purified by preparative HPLC (C18 reverse phase column, elution with a water/acetonitrile gradient with 0.1% trifluoroacetic acid). After lyophilization, the product **19a** (35 mg, 20%) was obtained as a white solid. ¹H NMR (DMSO-*d*₆): δ 8.09 (d, $J = 8.0$ Hz, 1H), 7.98 (d, $J = 8.4$ Hz, 1H), 7.85 (d, $J = 8.4$ Hz, 2H), 7.52 (t, $J = 7.6$ Hz, 2H), 7.38 (t, $J = 7.6$ Hz, 1H), 6.41 (s, 1H), 5.04 (s, 2H), 4.96 (m, 1H), 4.21 (dd, $J = 8.4$ Hz, $J = 3.9$ Hz, 1H), 4.14 (m, 1H), 4.05 (q, $J = 6.9$ Hz, 2H), 3.82 (m, 1H), 3.52 (m, 8H), 2.29 (m, 2H), 2.11–1.80 (m, 8H), 1.72 (m, 3H), 1.59 (m, 2H), 1.25 (m, 2H), 1.19 (t, $J = 6.8$ Hz, 3H). t_R (method b): 1.59 min. MS (ES) m/z : 696.5 (MH+).

6.2. Biology: Human P2Y₁₂ Recombinant Cell Membrane Binding Assay.¹⁷ As a source of P2Y₁₂, a membrane preparation was prepared from CHO cells with recombinant expression of the human P2Y₁₂ receptor according to standard procedures. To a 96-well microtiter plate, added were the following: (a) 24 μ L of assay buffer [10 mM 4-(2-hydroxyethyl)-1-piperazineethanesulfonic acid (HEPES), 138 mM NaCl, 2.9 mM KCl, 12 mM NaHCO₃, 1 mM EDTA-Na, and 0.1% BSA, pH 7.4], (b) 1 μ L of compound in DMSO, (c) 50 μ L of P2Y₁₂ CHO membrane (20 μ g/mL) and after 15 min at room temperature, and (d) 25 μ L of 1.61 nM [³³P]2-MeS-ADP (Perkin-Elmer NEN custom synthesis, specific activity ~2100 Ci/

mmol) made in assay buffer. The final concentration of [^{33}P]2-MeS-ADP was 0.8 nM, and the K_i value determined for [^{33}P]2-MeS-ADP was 0.5 nM. After 20 min of incubation at room temperature, samples were transferred and aspirated to 96-well microtiter filterplates (Millipore HTS GF/B) and prewetted for 20 min with 300 μL of stop buffer (10 mM HEPES, 138 mM NaCl, pH 7.4). After they were washed four times with 400 μL /well of stop buffer, the filters were air-dried overnight. After the addition of 0.1 mL of Microscint 20 Scintillation Fluid (Perkin-Elmer #6013621), the filter plates were incubated for 2 h at room temperature and counted in a Microbeta Scintillation Counter. The binding of compound is expressed as a % inhibition of specific binding, defined by subtraction of the background with 1 mM ADP. K_i values were calculated from the IC_{50} values using the Cheng-Prusoff equation assuming binding to a single binding site and were averaged from at least triplicate determination. The mean K_i value of the positive control used for each run was 0.4 μM , and the standard error of the mean (SEM) for this standard compound was $\pm 0.016 \mu\text{M}$ ($n = 61$).

6.2.1. Inhibition of Human Platelet Aggregation. **6.2.1.1. hPRP Preparation.** Human whole blood was from the Sanofi-Aventis in-house blood donor service. The protocol was approved by the local ethics committee, and all blood donors signed informed consent. Whole blood was collected from healthy volunteers using 20 mL syringes containing 2 mL of acid-citrate-dextrose solution (ACD-A) (for 96-well assays) or 2 mL of buffered citrate (for the light transmission aggregometry, Born method). The anticoagulated whole blood was transferred into 15 mL polypropylene conical tubes (10 mL per tube). The tubes were centrifuged for 15 min at room temperature at 150g (for 96-well assays) or at 340g (for the Born method), leading to a supernatant of hPRP. The hPRP layer was collected from each tube and pooled for each donor. The platelet concentration was determined using a Coulter counter. The 15 mL tubes containing the pellet of cellular components were centrifuged again for 10 min at 1940g, leaving a supernatant of platelet poor plasma (PPP). The PPP was collected for each donor. The PRP was diluted with PPP to a final concentration of 3×10^{-8} platelets/mL with the PPP.

6.2.1.2. IPs Preparation. IPs were obtained by centrifugation of PRP at 430g for 20 min at room temperature. The resulting platelet pellet was dissolved in a modified Tyrode's buffer containing 145 mM NaCl, 5 mM KCl, 0.1 mM $\text{MgCl}_2 \cdot 6\text{H}_2\text{O}$, 5.5 mM glucose, and 15 mM Hepes. The buffer was adjusted to pH 7.4. Platelets were counted and adjusted to 300×10^{-3} platelets/ μL . To 320 μL of IPs, 20 μL of CaCl_2 (final concentration, 0.5 mM) was added and incubated at 37 °C for 2 min before adding 20 μL of fibrinogen (final concentration, 1 mg/mL). The respective P2Y₁₂ antagonist was added (20 μL) and incubated, and the response to platelet activating agonists (20 μL) was recorded.

6.2.1.3. Human Platelet Aggregation 96-Well Assay.¹⁰ The human platelet aggregation assay was performed in 96-well plates using a microtiter plate reader (SpectraMax Plus 384 with SoftMax Pro software from Molecular Devices). In the plate, 15 μL of test compound at 10 \times final concentration in NaCl was mixed with 120 μL of fresh hPRP and incubated for 5 min. Following that incubation period, 15 μL of 40 μM ADP was added to the reaction mix, leading to a final concentration of 4 μM ADP. The plates were then transferred to the microplate reader, and aggregation was measured over 20 min. The instrument settings include the following: absorbance at 650 nm, run time 20 min with readings in 1 min intervals, and 50 s of shaking between readings, all performed at 37 °C. Results of the assay are expressed as % inhibition and are calculated using the AUC of the absorbance over 20 min. The IC_{50} values were averaged from at least triplicate determination. The mean value of the positive control used for each run was 0.27 μM , and the SEM for this standard compound was $\pm 0.026 \mu\text{M}$ ($n = 96$).

6.2.1.4. Human Platelet Aggregation Assay Light Transmission Aggregometry (Born Method).¹⁰ The human platelet aggregation assay was performed in single use cuvettes using the platelet aggregation profiler (PAP-8, Bio/Data corporation, Horsham, PA). In the assay cuvette, 4 μL of the test compound at 100 \times final concentration in DMSO was mixed with 392 μL of fresh hPRP and

incubated for 2 min at 37 °C with 1.200 rpm stirring. Following that incubation period, 4 μL of a 250 μM ADP solution was added to the reaction mix, leading to a final concentration of 2.5 μM ADP. After that, aggregation was measured over 6 min at 37 °C with 1.200 rpm stirring. Results of the assay are expressed as % inhibition and are calculated using the AUC of the absorbance over 6 min. The IC_{50} values were averaged from at least triplicate determination. The determination of the activity on ADP-, Col-, and Thr-induced aggregation in IPs was performed analogously. The final concentration of ADP was 10 μM , of Col was 1 $\mu\text{g}/\text{mL}$, and of Thr was 0.1 U/mL.

6.3. Computational Procedures: Homology Modeling and Molecular Docking. A homology model of the P2Y₁₂ receptor was generated using the crystal structure of the CXCR4 (PDB: 1odu) as the structural template. Sequence alignment and 3D model generation were performed using the software Prime (Prime, v2.2, Schrödinger, LLC, New York, NY). Molecular docking was performed with the Induced Fit Docking procedure²² based on Glide v5.7 (Glide, v5.7, Schrödinger, LLC) and Prime v2.2, as implemented in the Schrödinger package.

6.3.1. Generation of 3D Ligand Alignments. For the generation of multiple ligand 3D superimpositions, we used the MARS approach,²¹ which is based on the pairwise alignment of all molecules within the data set using the software tool ROCS.²³

6.3.2. Generation of 3D QSAR Models. Default settings were used for CoMFA and CoMSIA in Sybyl²⁴ if not otherwise indicated. Steric and electrostatic energies in CoMFA were calculated at grid points with 2 Å spacing, a positively charged carbon atom, and a distance-dependent dielectric constant with MMFF94 charges. For CoMSIA, steric, electrostatic, hydrophobic, donor, and acceptor fields were built using a Gaussian distance-dependent function. Cross-validated analyses were run using SAMPLS (LOO) or 10 cross-validation groups (LNO) with random selection of group members.

■ ASSOCIATED CONTENT

📄 Supporting Information

Experimental data for selected compounds 17–20 and additional biological characterization data. This material is available free of charge via the Internet at <http://pubs.acs.org>.

■ AUTHOR INFORMATION

✉ Corresponding Author

*E-mail: Marc.Nazare@sanofi.com.

Notes

The authors declare no competing financial interest.

■ ACKNOWLEDGMENTS

We thank A. Sihorsch, M. Kämmerer-Dienst, C. Prosser, S. Herok, D. Thorn, H. Krause, G. Sibenhorn, S. Stamm, A. Haber, F. Hopfinger, M. Pfeiffer, and R. Katzenmeier for their excellent technical assistance.

■ ABBREVIATIONS USED

ACD-A, acid-citrate-dextrose solution; ADP, adenosine diphosphate; AUC, area under curve; CHO, Chinese hamster ovary cell; Col, collagen; CoMFA, comparative molecular field analysis; CoMSIA, comparative molecular similarity index analysis; CXCR4, C-X-C chemokine receptor type 4; EC, extracellular loop; EDC, 1-ethyl-3-(3-dimethylaminopropyl)-carbodiimide hydrochloride; HATU, *O*-(7-azabenzotriazol-1-yl)-*N,N,N',N'*-tetramethyluronium hexafluorophosphate; HEPES, 4-(2-hydroxyethyl)-1-piperazineethanesulfonic acid; HOBt, 1-hydroxybenzotriazole; IP, isolated platelets; MARS, multiple alignments by ROCS-based similarity; ND, not determined; P2Y₁, P2Y purinoceptor 1; P2Y₁₂, P2Y purinoceptor 12; PI3K, phosphatidylinositol 3-kinase; hPRP, human

platelet-rich plasma; Thr, thrombin; TM, transmembrane domain; TOTU, O-((ethoxycarbonyl)cyanomethyleneamino)-N,N,N',N'-tetramethyluronium tetrafluoroborate; Z, Cbz benzoyloxy-carbonyl

REFERENCES

- (1) Gachet, C. ADP receptors of platelets and their inhibition. *Thromb. Haemostasis* **2001**, *86*, 222–232.
- (2) (a) Dangelmaier, C.; Jin, J.; Smith, J. B.; Kunapuli, S. P. Potentiation of thromboxane A₂-induced platelet secretion by Gi signaling through the phosphoinositide-3 kinase pathway. *Thromb. Haemostasis* **2001**, *85*, 341–348. (b) Cattaneo, M. Advances in antiplatelet therapy: overview of new P2Y₁₂ receptor antagonists in development. *Eur. Heart J. Suppl.* **2008**, *10* (Suppl. 1), I33–I37. (c) Cattaneo, M. ADP receptors: Inhibitory strategies for antiplatelet therapy. *Drug News Perspect.* **2006**, *19*, 253–259. (d) Cattaneo, M. P2Y₁₂ receptor antagonists: A rapidly expanding group of antiplatelet agents. *Eur. Heart J.* **2006**, *27*, 1010–1012.
- (3) (a) Dogne, J. M.; de Leval, X.; Benoit, P.; Delarge, J.; Masereel, B.; David, J. L. Recent advances in antiplatelet agents. *Curr. Med. Chem.* **2002**, *9*, 577–589. (b) Ingall, A. H.; Dixon, J.; Bailey, A.; Coombs, M. E.; Cox, D.; McNally, J. I.; Hunt, S. F.; Kindon, N. D.; Teobald, B. J.; Willis, P. A.; Humphries, R. G.; Leff, P.; Clegg, J. A.; Smith, J. A.; Tomlinson, W. Antagonists of the platelet P2T receptor: A novel approach to antithrombotic therapy. *J. Med. Chem.* **1999**, *42*, 213–220. (c) Storey, R. F. Biology and pharmacology of the platelet P2Y₁₂ receptor. *Curr. Pharm. Des.* **2006**, *12*, 1255–1259. (d) Nicholas, R. A. Identification of the P2Y(12) receptor: A novel member of the P2Y family of receptors activated by extracellular nucleotides. *Mol. Pharmacol.* **2001**, *60*, 416–420. (e) Dorsam, R. T.; Kunapuli, S. P. Central role of the P2Y₁₂ receptor in platelet activation. *J. Clin. Invest.* **2004**, *113*, 340–345.
- (4) (a) Judge, H. M.; Buckland, R. J.; Sugidachi, A.; Jakubowski, J. A.; Storey, R. F. Relationship between degree of P2Y₁₂ receptor blockade and inhibition of P2Y₁₂-mediated platelet function. *Thromb. Haemostasis* **2010**, *103*, 1210–1217. (b) Andre, P.; Delaney, S. M.; LaRocca, T.; Vincent, D.; DeGuzman, F.; Jurek, M.; Koller, B.; Phillips, D. R.; Conley, P. B. P2Y₁₂ regulates platelet adhesion/activation, thrombus growth, and thrombus stability in injured arteries. *J. Clin. Invest.* **2003**, *112*, 398–406.
- (5) (a) Savi, P.; Herbert, J.-M. Clopidogrel and ticlopidine: P2Y₁₂ adenosine diphosphate-receptor antagonists for the prevention of atherothrombosis. *Semin. Thromb. Hemostasis* **2005**, *31*, 174–183. (b) Hollopeter, G.; Jantzen, H. M.; Vincent, D.; Li, G.; England, L.; Ramakrishnan, V.; Yang, R. B.; Nurden, P.; Nurden, A.; Julius, D.; Conley, P. B. Identification of the platelet ADP receptor targeted by antithrombotic drugs. *Nature* **2001**, *409*, 202–207. (c) CAPRIE Steering Committee (CAPRIE). A randomised, blinded, trial of clopidogrel versus aspirin in patients at risk of ischaemic events. *Lancet* **1996**, *348*, 1329–1339; (d) The Clopidogrel in Unstable Angina to Prevent Recurrent Events Trial Investigators (CURE). Effects of Clopidogrel in Addition to Aspirin in Patients with Acute Coronary Syndromes without ST-Segment Elevation. *N. Engl. J. Med.* **2001**, *345*, 494–502.
- (6) (a) Savi, P.; Pereillo, J. M.; Uzabiaga, M. F.; Combalbert, J.; Picard, C.; Maffrand, J. P.; Pascal, M.; Herbert, J.-M. Identification and biological activity of the active metabolite of clopidogrel. *Thromb. Haemostasis* **2000**, *84*, 891–896. (b) Meadows, T. A.; Bhatt, D. L. Clinical aspects of platelet inhibitors and thrombus formation. *Circ. Res.* **2007**, *100*, 1261–1275. (c) Savi, P.; Zacharyus, J. L.; Delesque-Touchard, N.; Labouret, C.; Hervé, C.; Uzabiaga, M. F.; Pereillo, J. M.; Culouscou, J. M.; Bono, F.; Ferrara, P.; Herbert, J.-M. The active metabolite of Clopidogrel disrupts P2Y₁₂ receptor oligomers and partitions them out of lipid rafts. *Proc. Natl. Acad. Sci. U.S.A.* **2006**, *103*, 11069–11074. (d) Algaier, I.; Jakubowski, J. A.; Asai, F.; Von Kügelgen, I. Interaction of the active metabolite of prasugrel, R-138727, with cysteine 97 and cysteine 175 of the human P2Y₁₂ receptor. *J. Thromb. Haemostasis* **2008**, *6*, 1908–1914.
- (7) (a) Huber, K.; Hamad, B.; Kirkpatrick, P. Fresh from the pipeline. Ticagrelor. *Nat. Rev. Drug Discovery* **2011**, *10*, 255–256. (b) Gurbel, P. A.; Kereiakes, D. J.; Tantry, U. S. Ticagrelor for the treatment of arterial thrombosis. *Expert Opin. Pharmacother.* **2010**, *11*, 2251–2259.
- (8) (a) Ueno, M.; Rao, S. V.; Angiolillo, D. J. Elinogrel: Pharmacological principles, preclinical and early phase clinical testing. *Future Cardiol.* **2010**, *6*, 445–453. (b) Oestreich, J. H. Elinogrel, a reversible P2Y₁₂ receptor antagonist for the treatment of acute coronary syndrome and prevention of secondary thrombotic events. *Curr. Opin. Invest. Drugs* **2010**, *11*, 340–348. (c) Berger, J. S.; Roe, M. T.; Gibson, C. M.; Kilaru, R.; Green, C. L.; Melton, L.; Blankenship, J. D.; Metzger, D. C.; Granger, C. B.; Gretler, D. D.; Grines, C. L.; Huber, K.; Zeymer, U.; Buszman, P.; Harrington, R. A.; Armstrong, P. W. Safety and feasibility of adjunctive antiplatelet therapy with intravenous elinogrel, a direct-acting and reversible P2Y₁₂ ADP-receptor antagonist, before primary percutaneous intervention in patients with ST-elevation myocardial infarction: The Early Rapid Reversal of Platelet Thrombosis with Intravenous Elinogrel before PCI to Optimize REperfusion in Acute Myocardial Infarction (ERASE MI). *Am. Heart J.* **2009**, *158*, 998–1004.
- (9) (a) Bryant, J.; Post, J. M.; Alexander, S.; Wang, Y. X.; Kent, L.; Schirm, S.; Tseng, J. L.; Subramanyam, B.; Buckman, B.; Islam, I.; Yuan, S.; Sullivan, M. E.; Snider, M.; Morser, J. Novel P2Y₁₂ adenosine diphosphate receptor antagonists for inhibition of platelet aggregation (I): in vitro effects on platelets. *Thromb. Res.* **2008**, *122*, 523–532. (b) Post, J. M.; Alexander, S.; Wang, Y. X.; Vincelette, J.; Vergona, R.; Kent, L.; Bryant, J.; Sullivan, M. E.; Dole, W. P.; Morser, J.; Subramanyam, B. Novel P2Y₁₂ adenosine diphosphate receptor antagonists for inhibition of platelet aggregation (II): Pharmacodynamic and pharmacokinetic characterization. *Thromb. Res.* **2008**, *122*, 533–540. (c) Wang, Y. X.; Vincelette, J.; da Cunha, V.; Martin-McNulty, B.; Mallari, C.; Fitch, R. M.; Alexander, S.; Islam, I.; Buckman, B. O.; Yuan, S.; Post, J. M.; Subramanyam, B.; Vergona, R.; Sullivan, M. E.; Dole, W. P.; Morser, J.; Bryant, J. A novel P2Y(12) adenosine diphosphate receptor antagonist that inhibits platelet aggregation and thrombus formation in rat and dog models. *Thromb. Haemostasis* **2007**, *97*, 847–855.
- (10) (a) Cattaneo, M. Light transmission aggregometry and ATP release for the diagnostic assessment of platelet function. *Semin. Thromb. Hemostasis* **2009**, *35*, 158–167. (b) Breet, N. J.; van Werkum, J. W.; Bouman, H. J.; Kelder, J. C.; Ruven, H. J. T.; Bal, E. T.; Deneer, V. H.; Harmsze, A. M.; van der Heyden, J. A. S.; Rensing, B. J. W. M.; Suttorp, M. J.; Hackeng, C. M.; ten Berg, J. M. Comparison of Platelet Function Tests in Predicting Clinical Outcome in Patients Undergoing Coronary Stent Implantation. *J. Am. Med. Assoc.* **2010**, *303*, 754–762. (c) Jakubowski, J. A.; Li, Y. G.; Small, D. S.; Payne, C. D.; Tomlin, M. E.; Luo, J.; Winters, K. J. A comparison of the VerifyNow P2Y₁₂ point-of-care device and light transmission aggregometry to monitor platelet function with prasugrel and clopidogrel: An integrated analysis. *J. Cardiovasc. Pharmacol.* **2010**, *56*, 29–37.
- (11) (a) Parlow, J. J.; Burney, M. W.; Case, B. L.; Girard, T. J.; Hall, K. A.; Hiebsch, R. R.; Huff, R. M.; Lachance, R. M.; Mischke, D. A.; Rapp, S. R.; Woerndle, R. S.; Ennis, M. D. Piperazinyl-glutamate-pyridines as potent orally bioavailable P2Y₁₂ antagonists for inhibition of platelet aggregation. *Bioorg. Med. Chem. Lett.* **2009**, *19*, 4657–4663. (b) Parlow, J. J.; Burney, M. W.; Case, B. L.; Girard, T. J.; Hall, K. A.; Harris, P. K.; Hiebsch, R. R.; Huff, R. M.; Lachance, R. M.; Mischke, D. A.; Rapp, S. R.; Woerndle, R. S.; Ennis, M. D. Part II: Piperazinyl-glutamate-pyridines as potent orally bioavailable P2Y₁₂ antagonists for inhibition of platelet aggregation. *Bioorg. Med. Chem. Lett.* **2010**, *20*, 1388–1394. (c) Parlow, J. J.; Burney, M. W.; Case, B. L.; Girard, T. J.; Hall, K. A.; Harris, P. K.; Hiebsch, R. R.; Huff, R. M.; Lachance, R. M.; Mischke, D. A.; Rapp, S. R.; Woerndle, R. S.; Ennis, M. D. Piperazinyl glutamate pyridines as potent orally bioavailable P2Y₁₂ antagonists for inhibition of platelet aggregation. *J. Med. Chem.* **2010**, *53*, 2010–2037.
- (12) Part of this work has been patented by the authors: (a) Nazare, M.; Zech, G.; Goerlitzer, J.; Just, M.; Weiss, T.; Hessler, G.; Czechtizky, W.; Ruf, S. Pyrazole-carboxamide derivatives as P2Y₁₂ antagonist. WO2009080227, 2009. (b) Nazare, M.; Zech, G.; Just, M.;

Weiss, T.; Hessler, G.; Kohlmann, M. Heterocyclic pyrazole-carboxamides as P2Y12 antagonists. WO2009080226, 2009.

(13) (a) Caroff, E.; Hilpert, K.; Meyer, E. 2-Phenyl-6-aminocarbonyl-pyrimidine derivatives and their use as P2Y12 receptor antagonists. WO2008050301, 2008. (b) Caroff, E.; Hilpert, K.; Meyer, E. Preparation of N-(2-pyridylcarbonyl) amino acid piperazides and their use as P2Y12 receptor antagonists. WO2008044217, 2008. (c) Caroff, E.; Fretz, H.; Hilpert, K.; Houille, O.; Hubler, F.; Meyer, E. Pyrimidine derivatives and their use as P2Y12 receptor antagonists. WO2006114774, 2006.

(14) Deflorian, F.; Jacobson, K. A. Comparison of three GPCR structural templates for modeling of the P2Y12 nucleotide receptor. *J. Comput.-Aided. Mol. Des.* **2011**, *25*, 329–338.

(15) Wheatley, M.; Wootten, D.; Conner, M. T.; Simms, J.; Kendrick, R.; Logan, R. T.; Poyner, D. R.; Barwell, J. Lifting the lid on GPCRs: The role of extracellular loops. *Br. J. Pharmacol.* **2012**, *165*, 1688–1703.

(16) Hao, M.; Li, Y.; Wang, Y.; Yan, Y.; Zhang, S.; Li, G.; Yang, L. Combined 3D-QSAR, Molecular Docking, and Molecular Dynamics Study on Piperazinyl-Glutamate-Pyridines/Pyrimidines as Potent P2Y12 Antagonists for Inhibition of Platelet Aggregation. *J. Chem. Inf. Model.* **2011**, *51*, 2560–2572.

(17) (a) Takasaki, J.; Kamohara, M.; Saito, T.; Matsumoto, M.; Matsumoto, S.; Ohishi, T.; Soga, T.; Matsushime, H.; Furuichi, K. Molecular cloning of the platelet P2T(AC) ADP receptor: pharmacological comparison with another ADP receptor, the P2Y(1) receptor. *Mol. Pharmacol.* **2001**, *60*, 432–439. (b) Savi, P.; Labouret, C.; Delesque, N.; Guette, F.; Lupker, J.; Herbert, J. M. P2Y(12), a new platelet ADP receptor, target of clopidogrel. *Biochem. Biophys. Res. Commun.* **2001**, *283*, 379–383.

(18) (a) Mao, Y.; Zhang, L.; Jin, J.; Ashby, B.; Kunapuli, S. P. Mutational analysis of residues important for ligand interaction with the human P2Y(12) receptor. *Eur. J. Pharmacol.* **2010**, *644*, 10–16. (b) Hoffmann, K.; Sixel, U.; Di Pasquale, F.; von Kügelgen, I. Involvement of basic amino acid residues in transmembrane regions 6 and 7 in agonist and antagonist recognition of the human platelet P2Y(12)-receptor. *Biochem. Pharmacol.* **2008**, *76*, 1201–1213.

(19) (a) Graff, J.; Klinkhardt, U.; Harder, S. Pharmacodynamic profile of antiplatelet agents: Marked differences between single versus costimulation with platelet activators. *Thromb. Res.* **2004**, *113*, 295–302. (b) Storey, R. F.; Newby, L. J.; Heptinstall, S. Effects of P2Y(1) and P2Y(12) receptor antagonists on platelet aggregation induced by different agonists in human whole blood. *Platelets* **2001**, *12*, 443–447. (c) Sugidachi, A.; Asai, F.; Yoneda, K.; Iwamura, R.; Ogawa, T.; Otsuguro, K.; Koike, H. Antiplatelet action of R-99224, an active metabolite of a novel thienopyridine-type G(i)-linked P2T antagonist, CS-747. *Br. J. Pharmacol.* **2001**, *132*, 47–54.

(20) (a) Huang, J.; Driscoll, E. M.; Gonzales, M. L.; Park, A. M.; Lucchesi, B. R. Prevention of arterial thrombosis by intravenously administered platelet P2T receptor antagonist AR-C69931MX in a canine model. *J. Pharmacol. Exp. Ther.* **2000**, *295*, 492–499. (b) Soloviev, M. V.; Okazaki, Y.; Harasaki, H. Whole blood platelet aggregation in humans and animals: A comparative study. *J. Surg. Res.* **1999**, *82*, 180–187.

(21) Klabunde, T.; Giegerich, C.; Evers, A. MARS: Computing three-dimensional alignments for multiple ligands using pairwise similarities. *J. Chem. Inf. Model.* **2012**, *52*, 2022–2030.

(22) Sherman, W.; Day, T.; Jacobson, M. P.; Friesner, R. A.; Farid, R. Novel procedure for modeling ligand/receptor induced fit effects. *J. Med. Chem.* **2006**, *49*, 534–553.

(23) Rush, T. S., III; Grant, J. A.; Mosyak, L.; Nicholls, A. A shape-based 3-D scaffold hopping method and its application to a bacterial protein-protein interaction. *J. Med. Chem.* **2005**, *48*, 1489–1495.

(24) SYBYL Molecular Modelling Package, Version 8.0; Tripos: St. Louis, MO, 2009.